4-2016

Phosphorus Adsorption through Engineered Biochars Produced from Local Waste Products

Peter Ogonek
University of Dayton

Phosphorus Adsorption through Engineered Biochars Produced from Local Waste Products

Honors Thesis

Peter Joshua Ogonek

Department: Civil and Environmental Engineering

Advisor: Denise Taylor, Ph.D., P.E.

May 2016

Phosphorus Adsorption through Engineered Biochars Produced from Local Waste Products

Honors Thesis

Peter Ogonek

Department: Civil and Environmental Engineering and Engineering Mechanics

Advisor: Denise Taylor, Ph.D., P.E.

May 2016

Abstract

Phosphorus contained in agricultural runoff is a major anthropogenic contributor to harmful algal blooms (HABs). Biochars are carbon-based materials produced from the pyrolysis of waste biomass that have the potential to amend soils and remediate inorganic and organic contaminants from water. Engineered biochars tailored to adsorb phosphorus from water could reduce the availability of the nutrient in agricultural runoff, reducing the size and frequency of HABs. This study observed the phosphorus adsorption properties of engineered biochars produced from two source materials, oak sawdust and cornstalk residue, and being unmodified, acid-rinsed, or loaded with magnesium prior to pyrolysis, creating acid-rinsed, unmodified, and magnesium oxide biochars. Results indicate that the unmodified biochars released phosphates into solution, hinting at a potential agricultural soil amendment similar to older slash and burn methods of burning and burying crop residue. Magnesium-loaded biochars removed ~99% of 30 mg/L phosphate with 40 mL of solution and 0.1g of biochar. Further adsorption testing of the magnesium biochars showed a maximum adsorption capacity of 174 mg phosphate/g biochar for the sawdust-based biochar and 249.6 mg phosphate/g biochar for the cornstalk-based biochar. The sawdust biochar fit well with both the Freundlich and Langmuir isotherm models, slightly favoring the Langmuir isotherm, which suggests linear monolayer adsorption as the major adsorption mechanism. The cornstalk-based biochar did not fit either isotherm model particularly well, which suggests that the cornstalk biochar is influenced by other adsorption mechanisms.

Acknowledgements

To Dr. Denise Taylor, my academic advisor, mentor, and who pushed me to excel,
Dr. Kenya Crosson, who mentored me through my research and influenced my studies,
The University of Dayton Civil Engineering Department,
The University of Dayton Honors Department, who made this wonderful opportunity possible,
And my family, who made me the person I am today and fostered a lifelong love of learning.

TABLE OF CONTENTS

Abstract..... Title Page
List of Figures iii
List of Tables..... iv
List of Abbreviations..... iv
1 Introduction..... 1
2 Literature review..... 2
2.1 Eutrophication and harmful algal blooms..... 2
2.2 Biochars..... 4
2.2.1 Biochar characteristics..... 4
2.2.2 Biochar production..... 5
2.2.3 Potential Applications..... 7
3 Proposed solution..... 12
4 Materials and methods..... 13
4.1 Raw materials..... 13
4.1.1 Cornstalk residue..... 13
4.1.2 Oak sawdust..... 13
4.1.3 Biochar pre-treatment..... 14
4.2 Experimental methods..... 16
4.2.1 Pyrolysis trials..... 16
4.2.2 Phosphorus adsorption and desorption..... 17
4.3 Analytical methods..... 19
5 Results and Discussion..... 21
5.1 Pyrolysis yields..... 21
5.2 Biochar characterization..... 23
5.2.1 Bulk Density..... 23
5.2.2 Interactions with water..... 24
5.2.3 Visual characteristics..... 26
5.3 Phosphate Adsorption Results..... 26
5.3.1 Desorption of phosphates..... 26
5.3.2 Phosphate adsorption tests..... 28
5.4 Adsorption mechanisms and biochar characteristics..... 32
5.4.1 Surface area and porosity..... 32
5.4.2 Adsorption characteristics of MgO biochars..... 33
5.5 Practical Applications..... 34
5.5.1 Biochar Production..... 34
5.5.2 Potential biochar applications..... 35
6 Conclusion..... 37
7 References..... 38
8 Appendices..... I

8.1 Detailed Experimental Methods I
8.1.1 General materials used: I
8.1.2 Pre-pyrolysis preparation I
8.1.3 Biochar Production II
8.1.4 Adsorption Trials III
8.2 Experimental Matrix for Adsorption Trials V
8.3 Data and Sample Calculations VI
8.3.1 Biochar Yield VI
8.3.2 Bulk Density VII
8.3.3 30 mg/L Phosphate Adsorption Screen VIII
8.3.4 Adsorption Trials IX
8.4 Pyrolysis Reactor XIII
8.4.1 Detailed pyrolysis reactor: XIII
8.4.2 Pyrolysis reaction schematic XIII

LIST OF FIGURES

Figure 2.1: Ohio River HAB advisory summary map 2
Figure 2.2: HAB extent in the Gulf of Mexico 3
Figure 4.1: Sample of cornstalk residue, as received 13
Figure 4.2: Prepared sawdust (left) and cornstalk residue (right) before pyrolysis 14
Figure 4.3: Cornstalk acid rinse with manual agitation 15
Figure 4.4: Loading cornstalk residue with MgCl salt using SI-300R orbital shaker 15
Figure 4.5: Steel reactor for pyrolysis trials 16
Figure 4.6a: Sawdust before pyrolysis, after pyrolysis, and after final production steps 16
Figure 4.6b: Enlarged image of final biochar products. 17
Figure 4.7: 50 mL Fisher Falcon tube, empty and with 40mL of 30 mg/L PO_4^{3-} Solution and 0.1 g CMgO 17
Figure 4.8: Big SHOT hybridization oven used for adsorption isotherm experiments 18
Figure 5.1: Biochar yield by mass for different engineered biochars 21
Figure 5.2: Bulk density of prepared biochars vs raw materials 23
Figure 5.5a: Hydrophobic CMgO Figure 5.5b: Hydrophilic CA 25
Figure 5.4: SA (left) and SMgO (right), 15 minutes of settling after agitation 25
Figure 5.5: Highlighting the color variation in CA (left) and SA (right) 26
Fig. 5.6a: PO_4^{3-} release in RO water after 24h with RO interference error bars 27
Fig. 5.6b: PO_4^{3-} release in RO water after 24 h, enlarged 27
Figure 5.7: Removal efficiencies of biochars at 30 ppm PO_4^{3-} 28
Figure 5.8: 30 mg/L PO_4^{3-} adsorption capacity with variable mass SMgO and CMgO 29
Figure 5.9: Ce vs qe of CMgO and SMgO 30
Figure 5.10a: Linearized Freundlich isotherm model of SMgO and CMgO 31
Figure 5.10b: Linearized Associative Langmuir isotherm model of SMgO and CMgO 31
Figure 5.11: Multiple hearth kiln 35

LIST OF TABLES

Table 2.1: Production methods for biochars....6
Table 2.2: Biochar treatment methods and their effect on biochar characteristics....7
Table 2.3: Biochars used to remediate organic contaminants, and their effects....9
Table 2.4: Biochars used to remediate inorganic contaminants in soils and water....10
Table 4.1: Abbreviations for engineered biochars....14
Table 5.1: Removal efficiencies and q values at 30 ppm PO_4^{3-}....28
Table 5.2: Isotherm model constants[1]....31
Table 5.3: Surface area and pore characteristics of previous biochar studies....33

LIST OF ABBREVIATIONS

HAB –Harmful Algal Blooms

P-Phosphorus/phosphate

PO_4^{3-} -Phosphate

S -Sawdust

C -Cornstalk Residue

SP – Pristine, or unmodified (prior to pyrolysis) sawdust biochar

CP –Pristine, or unmodified (prior to pyrolysis) cornstalk biochar

SA –Acid-rinsed sawdust biochar

CA –Acid-rinsed cornstalk residue biochar

SMgO –Magnesium-loaded/magnesium oxide sawdust biochar

CMgO –Magnesium-loaded/magnesium oxide cornstalk residue biochar

RO –Reverse Osmosis

HTC –Hydrothermal Carbonization

SA –Surface Area (in context of adsorption mechanisms)

PV –Pore volume

Ppm –Parts per million (same as mg/L)

TEM –Transmission electron microscopy

BET -Brunauer–Emmett–Teller adsorption theory

1 INTRODUCTION

Harmful algal blooms (HABs) are quickly becoming a major environmental concern for global surface waters. The size and intensity of HABs increase every year, causing drinking water or general water advisories and environmental damage. A major contributor to these algal blooms is phosphorus from agricultural runoff, providing a catalyst for accelerated algal growth. One potential method to reduce the amount of phosphorus entering surface waters is with biochars. Biochars are an up and coming environmental remediation tool that are generally inexpensive to produce and share many physical and chemical similarities to activated carbons, which are commonly used in water and wastewater treatment facilities. A more detailed description of harmful algal blooms and biochars can be found in the Literature Review (section 2) starting on pg. 2.

The solution proposed in this thesis to remove phosphorus from an aqueous solution is to use engineered biochars. Details for the proposed solution can be found in section 3, pg. 11.

Engineered biochars were prepared using three different production methods with two different source materials: unmodified biochar, acid-rinsed biochar, and magnesium-loaded biochar. Raw material was pyrolyzed after pretreatment. The engineered biochars produced in this thesis were evaluated for phosphate release into reverse osmosis (RO) water, phosphate removal from a phosphate concentration, and adsorption capacity for biochars that showed phosphate removal capabilities using batch reactors. The experimental setup, pretreatment methods, adsorption experiments, and analytical methods can be found in section 4, Materials and Methods, pg. 12.

The engineered biochars produced were characterized using physical and chemical properties including solid mass yield from pyrolysis, apparent density, interactions in water, and visual characteristics. Data gathered during adsorption was used to determine the removal efficiencies of the engineered biochars with a 30 mg/L phosphate solution. Biochars that displayed high removal efficiencies were further tested and put in Langmuir and Freundlich isotherm models to characterize the adsorption characteristics of the materials. Results and a detailed discussion of the results, including possible applications and scaling of biochar production, are included in section 5, Results and Discussion, starting on pg. 20. Conclusions of this thesis and future research directions are in section 6, pg. 35.

2 LITERATURE REVIEW

2.1 EUTROPHICATION AND HARMFUL ALGAL BLOOMS

Over the last few years, algal blooms in Ohio have been documented with an increasing frequency and intensity (Ohio EPA 2015). In August 2014, the City of Toledo issued a "Do Not Drink or Boil" advisory to residents serviced by the Toledo Water Treatment Plant, leaving 500,000 people in three counties of Ohio and parts of Michigan without a reliable source of drinking water. Dangerous levels of microcystin, cyanobacteria found naturally in water that proliferates through algal blooms, were found in the city's finished drinking water. A harmful algal bloom (HAB) located near Toledo's source water on Lake Erie caused an unexpected influx of the algal toxin and quickly rose to levels outside of acceptable treatment standards. Two days later, the advisory was lifted after adjustments were made to the treatment process that reduced the level of cyanobacteria to acceptable World Health Organization guidelines in all samples from the treatment plant and distribution system (US EPA 2015).

In addition to affecting drinking water supplies in Lake Erie, this cyanobacteria has created problems more recently along the Ohio River. In August of 2015, an algal bloom stretching over *600 miles* along the Ohio River, reaching the states of Illinois, Indiana, Kentucky, Ohio, and West Virginia, developed (Figure 2.1). This scale of algal bloom was unprecedented in this body of water, and precautionary statements and water advisories for recreational use and drinking water consumption were issued where necessary. Environmental agencies lifted these advisories in November 2015, when water sample tests showed that the HABs had subsided to an acceptable level (West Virginia BPD 2015).

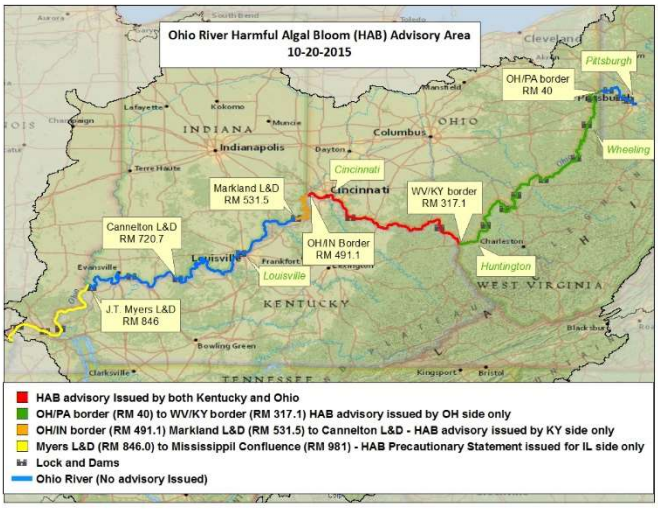

Figure 2.1: Ohio River HAB advisory summary map
Source: (ORSANCO, 2015)

While both of these cases happened in or around Ohio, they represent a much larger issue at hand. The Ohio River and over 3,225,000 km^2 of the U.S. that drains into the Mississippi River and into the Gulf of Mexico can have a profound effect on the surface waters along the Gulf Coast. (Rabalais et al. 2009) Any influx of algal-bloom enhancing pollution into the Gulf adds to an algal bloom that is currently, as of August 2015, measured at 5,052 square miles—larger than the states of Connecticut and Rhode Island combined (NOAA 2015) (Figure 2.2). These blooms are not just characterized by negatively affecting human health—many algal blooms are non-toxic to humans, but can still have negative environmental effects. Increased algal growth leads to an accelerated aging of a body of water, known as eutrophication, resulting in an eventual 'dead zone' where no aquatic life can live (Diaz and Rosenberg 2008; Rabalais et al. 2009). An economic cost is also associated with these algal blooms, with a 2009 analysis of eutrophication of U.S. freshwaters estimating algal blooms causing approximately $2.2 billion in economic damages, from increased water treatment costs to decreased lakefront property values (Dodds et al. 2009).

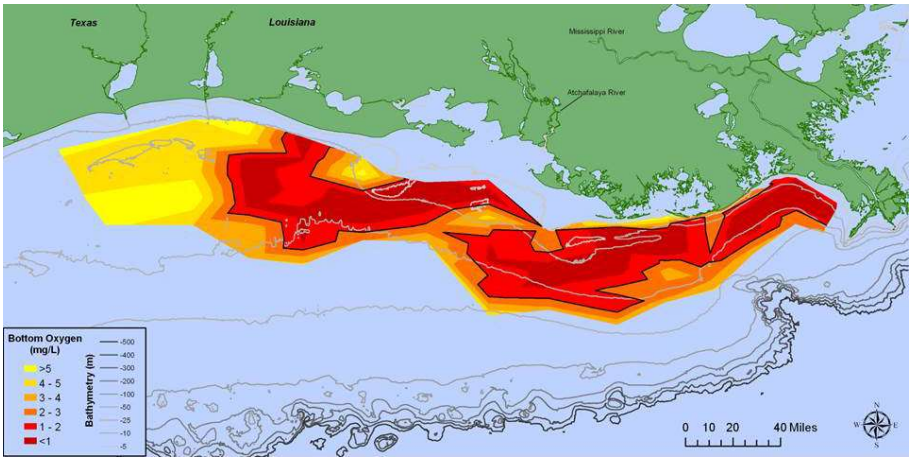

Figure 2.2: HAB extent in the Gulf of Mexico
(Source: NOAA)

These HABs have both human and natural causes, with increased anthropocentric stressors being directly linked to an increased frequency and intensity of these algal blooms throughout the globe (Rabalais et al. 2009). A major contribution to human-caused HABs is an increased nutrient content in surface waters. In many areas, phosphorus (P) or nitrogen (N) are the limiting factors of algal blooms (Carpenter et al. 1998; Daniel et al. 1998). A total P concentration of 0.02 mg/L causes increased algal growth, leading to accelerated eutrophication (Daniel et al. 1998) While point-sources of P and N are easily regulated and controlled, non-point sources of these nutrients are difficult to monitor. A major source of P non-point source pollution is agricultural runoff, stemming from excess fertilizer, animal wastes, and other agricultural runoff products (Carpenter et al. 1998). If the amount of P contained in agricultural fertilizer

runoff was limited, HABs where P is a limiting growth factor could be significantly reduced.

Various wastewater treatment techniques have been evaluated for their potential to remove P from agricultural runoff. Precipitation from metal salts, utilizing microorganisms, constructing wetlands, creating advanced biological processes, and adsorption have all been tested (De-Bashan and Bashan 2004). Adsorption is a particularly appealing process, as it can have a low initial cost if materials are gathered locally and inexpensively, can remove pollutants with very low concentrations, is simple to maintain, and most times environmentally friendly. Currently, many wastewater and water treatment adsorption processes uses activated carbon, an extremely effective adsorbent for a variety of contaminants, to remove materials from both an aqueous and gaseous solution. However, activated carbons can be prohibitively expensive to use in the large quantities needed for nonpoint source pollution, making them impractical for agricultural use. As such, Biochars, an inexpensive and environmentally friendly material, are a potential solution to controlling P discharge from agricultural runoff, limiting the amount of nutrients available for HABs.

2.2 BIOCHARS

Biochars are an up-and coming environmental remediation tool currently undergoing testing in a variety of situations. Biochars are a form of black carbon produced through heating organic, carbon-based materials to a high (200-900° C) temperature under limited oxygen conditions (Lehmann and Joseph 2009). Typical biochar production uses waste biomass products, such as agricultural waste products, algae used for water treatment, or wood byproducts such as sawdust, husks, and cherry stones. Historically, biochars have been observed in low-fertility or infertile areas to increase soil fertility and crop production. (Glaser et al. 2002) Recent studies have successfully used biochars for soil amendments, soil and water contaminant remediation, increased crop fertility, and mitigating greenhouse gas emissions (Ahmad et al. 2014; Beesley et al. 2011; Glaser et al. 2002; Kookana et al. 2011; Qian et al. 2015; Sohi et al. 2010). Many of these studies have involved tailoring locally gathered biochars through production temperature, pre-treatment acid washes or material loading, or post-treatment amendments to increase intended effects of the biochar (Ahmad et al. 2014; Mubarik et al. 2014; Qian et al. 2015; Roberts et al. 2015; Sun et al. 2015; Trakal et al. 2016; Zhang et al. 2012). Tailoring biochars from locally available bio-waste products to adsorb P from agricultural runoff is a potentially economical and material-efficient method to reduce nutrient content in surface waters, thereby reducing the amount of HABs limited by P.

2.2.1 Biochar characteristics

While the physical and chemical properties of biochars can be widely varied depending on source material and production methods, biochars have several key characteristics

making them suitable to tailor for specific purposes. Biochar composition consists of mainly carbon (70-80%), with other non-volatile trace minerals from source material contained within the char material, including essential nutrients (Anawar et al. 2015; Guo and Bi 2015; Huang et al. 2012). Like activated carbons, biochars have a high surface area and porosity. The macropore structure in biochars is inherited from the cellulose structure of the source material (Sohi et al. 2010), and surface area, governed primarily by micropores, is mostly affected by production temperature (Sohi et al. 2010). Other key characteristics of biochars that can be manipulated include: pH, surface charge, surface groups, volatile compound and ash content, water-holding capacity, bulk density, pore volume, and specific surface area (Anawar et al. 2015; Okimori et al. 2003; Sohi et al. 2010). The main production parameter that affects these characteristics is pyrolysis temperature, followed by heating rate, and feed composition, as the fundamental physical changes occurring are heat-dependent. (Lehmann and Joseph 2009; Sohi et al. 2010). Other parameters, including pretreatment of the biochars, can alter the characteristics, but are not as controllable and do not have as significant of an impact on biochar characteristics (Lehmann and Joseph 2009; Peacocke 1994)

2.2.2 Biochar production

The production of biochars occurs from the heating of carbon-based material, such as cornstalk, sawdust, or other organic waste materials, under no or limited oxygen conditions. Common production methods include pyrolysis or hydrothermal carbonization, heating raw materials in elevated pressure and temperature water. Production parameters including the biomass composition, reaction conditions, and the recovery of the final products all affect the yields and compositions of biochars (Peacocke 1994), but the effects of one single parameter are not currently well-defined (Lehmann and Joseph 2009). The largest influence on biochar properties are the composition of the biomass and reaction parameters (Lehmann and Joseph 2009). However, some industrial pretreatment methods can tailor biochars for specific purposes, such as adsorbing heavy metals, nutrients, or inorganic contaminants.

2.2.2.1 Pyrolysis

The production of biochars is similar in nature to activated carbon production for water treatment. Both materials use organic, carbon-based material and expose them to heat under low oxygen conditions to produce a carbonaceous material. Activated carbon typically has high production temperatures (>700-1000 °C) and has been activated through steam or chemicals at a high temperature (Boehm 1994). In comparison, biochar production occurs at a generally lower temperature (200-600 °C) and undergoes much simpler pre- or post-treatment processes to alter the chemical and physical characteristics of the material. Biochar production mechanisms usually involve the thermochemical decomposition of organic material at elevated temperatures under limited oxygen

conditions, a process known as pyrolysis. Hydrothermal Carbonization (HTC) is also a production method for biochars, exposing biochars to heat in water with an elevated pressure to keep water in the liquid form. See Table 2.1 for common production methods for biochars. Biochar production also produces synthesis gas (syngas), and a water-based bio-oil liquid, which can be used for heat, as fuel, food additives, or soil conditioner/fertilizers (Sohi et al. 2010). The fractions of biochar, syngas, and bio-oil produced are predominantly dependent on the production conditions (temperature, residence time) (Table 2.1), and can vary based on feedstock composition. While low-temperature HTC produces the highest yield of biochar, carbonaceous compounds produced under HTC are less stable than pyrolysis biochars (Mohan et al. 2014). As such, slow-pyrolysis produces favorable fractions of biochar, and is the best choice for any large-scale of production of biochars. Charcoal production has occurred for many years under pyrolysis or very similar conditions (Lehmann and Joseph 2009). Large-scale production of biochars under slow pyrolysis is feasible with modified charcoal kilns that are capable of producing multiple tons of charcoal over a period of several days to a week (Whitehead 1980; William H. Maxwell 1976; Wood et al. 2014) with theoretically similar biochar production efficiencies. (Kammen and Lew 2005)

Table 2.1: Production methods for biochars

	Process	*Temperature*	*Residence time*	*Bio-oil (%)*	*Biochar (%)*	*Syngas (%)*
Pyrolysis Variations	Fast	~500 °C 400-600	1-2s	75 (25% water)	12%	13%
	Intermediate	~500 °C 400-600	10-20s	50% (50% water)	25	25
	Slow	~500 °C 350-800	5 min - days	30% (70% water)	35 20-40%	35
	Gasification	>750 °C	5-20s	5% tar (5% water)	~10	85
	HTC	180-250	1-12h	N/A	30-60%	N/A

Source: (Lehmann and Joseph 2009; Mohan et al. 2014; Qian et al. 2015; Sohi et al. 2010)

2.2.2.2 Pretreatment methods

Although pyrolysis temperature and heating rate control the major factors influencing biochar characteristics, industrial treatment methods and novel treatment methods have been applied to successfully alter essential physical characteristics including total surface area (SA), total pore volume (PV), macro- and micro-pore composition, pore size and surface chemistry characteristics of biochars (Table 2.2). Similar to activated carbon production, biochars can be activated, increasing the total pore volume and micropore composition to enhance adsorption capacities of the material. This is typically done

physically through steam activation at high temperature post-pyrolysis, or chemically with materials such as zinc salts or phosphoric acid pre- or post-pyrolysis. Chemical activation is advantageous to use in biochar production as it is carried out in a single step and results in a greater production of porous structures, but may also have environmental implications from waste produced (Zhang et al. 2004). An activated biochar may have different adsorption qualities than unmodified biochar, and should be tested for P sorption/desorption in water.

In addition to chemical or physical activation, several novel techniques have been applied to change integral biochar characteristics (Table 2.2). Processes such as magnetization, creating metal oxides or zero-valent iron nanocomposites, or producing alkali-modified biochars can improve the performance of biochars over certain tasks, such as ion adsorption, amending acidic soils, or remediating contaminated soils. These treatment methods are typically performed pre-pyrolysis, influencing the structure of the biochar. Because of the negative charge of phosphates in solution, a Magnesium-loaded biochar, which should produce a positively-charge MgO biochar nanocomposite, will be tested with local source materials. (Zhang et al. 2012)

Table 2.2: Biochar treatment methods and their effect on biochar characteristics

Biochar produced	*Biochar treatment*	*Effect on biochar*	*Source*
Magnetic biochar	Co-precipitation with FeCl compounds	Decreased SA, PV High number of micropores Separated from solution easily	(Chen et al. 2011)
Alkali	Alkali Modification with NaOH	Alkaline biochar Greatly increased SA, cation exchange capacity	(Ding et al. 2015)
Zero-Valent Iron biochar	Reduction reaction performed in presence of BIOCHAR	Greatly reduced PV, SA Greatly increased pore size	(Han et al. 2015)
MgO-biochar	Biochar immersed in MgCl solution	MgO-biochar nanocomposites formed	(Yao et al. 2013b)
MgO-biochar	Feedstock bioaccumulation of MgO	MgO-biochar nanocomposites formed	(Zhang et al. 2012)
Acid-Modified biochar	Immersing source material with acids prior to heat application	Increased monolayer adsorption capacity, Introduction of carboxyl groups, Increased or decreased SA, PV	(Sun et al. 2015)

2.2.3 Potential Applications

The physical and chemical characteristics of biochars as well as their inexpensive production methods make them attractive materials for use in different situations. Varieties of biochars have been tested as an agricultural soil amendment to increase soil fertility and facilitate crop growth. In addition, the similarities of biochars to activated

carbons make them potential contaminant management tools in soil and water. Significant research has been conducted on the use of biochars for the treatment of organic contaminants and inorganic contaminants (mainly heavy metals or mining wastes). However, little literature exists for the use of biochars as a nutrient (P, N, etc.) adsorbent.

2.2.3.1 Biochars in agriculture

The concept of using biochars stem as a soil remediate for agricultural purposes can be traced back thousands of years through the *Terra Preta* soils of humid tropical areas, where pre-historic people used slash and burn techniques to increase soil fertility. Studies of these soils have found an abundance of soil organic matter and nutrients essential to soil fertility including N, P, and Ca, stemming from the incomplete combustion of plants, leading to charcoal mixed in with soils. (Glaser et al. 2002). While slash and burn techniques with crop residue or trees still experiences widespread use, this technique is not advisable. The *in-situ* burning of plants results in negative effects on soil physical properties and microbial populations, and can be economically unfeasible, particularly in the slashing and burning of trees, whereas trees are more valued in their use as a construction material or charcoal for general purposes. (Dooley and Treseder 2012; Glaser et al. 2002). Biochars produced from waste biological matter under controlled conditions and subsequently added to agricultural soils is much safer than traditional slash and burn techniques (Qayyum et al. 2015), and is much more economically feasible.

Recent studies have examined the potential of biochars to increase crop yield in a variety of soil conditions. Biochar has been noted to increase the soil fertility, pH in acidic soils, soil cation exchange capacity ,and improve soil microbial activity and nutrient retention (Qian et al. 2015). Laghari et al. (2015) studied the use of fast-pyrolysis biochars under a variety of pyrolysis conditions to amend the Kubuqi Desert soil with 5% by mass of produced biochar. Using sorghum as a test crop, it was determined that crop yield increased by up to 30% with a pyrolysis temperature of 700 degrees C. The fast-pyrolysis biochar improved soil organic matter, cation exchange capacity, and plant nutrient content significantly (Laghari et al. 2015). HTC-produced biochar, with an addition of compost, was found to increase the pH of acidic soils, in one case from 4.5 to 6.1 (Qayyum et al. 2015). Roberts et al. utilized a macroalgae cultivated from wastewater that contained trace elements including As, Cd, Cr, Cu, and Pb to produce a biochar under slow pyrolysis that when added to low-quality soil increased the radish yield by 30-40% (Roberts et al. 2015). A study using MgO enhanced biochar to sorb P and subsequently tested its application in soils as a slow-release fertilizer. Much of the P captured onto the MgO biochar was able to desorb P into an aqueous solution as a slow-release fertilizer, increasing plant growth rate (Yao et al. 2013a). Using a biochar that has removed P from agricultural runoff as a fertilizer in cropland has the potential to

create a closed-loop biochar system that can significantly reduce both the amount of P contained in agricultural runoff and the amount required for adequate crop growth.

2.2.3.2 Biochars for contaminant management

The similarities between biochars and activated carbons have led to research in using biochars to remediate organic contaminants, both in soil and water. The high surface area and microporosity allows for adsorption of organic contaminants contained in water (Ahmad et al. 2014). Generally, production temperatures >400 °C increase the adsorption capacity of organic pollutants onto biochars. A higher production temperature generally increases the carbonized fraction of the biochar, and the surface of the biochar surfaces become less polar and more aromatic. The adsorption mechanisms shift from linear competitive partition adsorption to competitive adsorption onto complete carbonized fractions of the material (Ahmad et al. 2014; Beesley et al. 2011; Kuppusamy et al. 2016). Application of biochars in soils containing organic contaminants can potentially reduce or suppress contaminant biodegradation and the leaching of the contaminant into groundwater sources (Jones et al. 2011). Table 2.3 below gives a brief overview of several types of organic contaminants and biochars used to successfully remove them from an aqueous phase or immobilize/reduce their bioavailability in soils.

Table 2.3: Biochars used to remediate organic contaminants, and their effects

Media	*Biochar*	*Contaminant*	*Results*	*Source*
Soil	Hardwood	Polycyclic aromatic hydrocarbons	Adsorption and biodegradation	(Beesley et al. 2010)
	Pine wood	Phenanthrene	Entrapment in pores	(Zhang et al. 2010)
	Dairy manure	Atrazine	Sorption of Atrazine	(Cao et al. 2011)
	Bamboo	Pentachlorophenol	Reduced leaching from diffusion and partition adsorption	(Xu et al. 2012)
Water	Pine needles	m-Dinitrobenzene	Adsorption of m-Dinitrobenzene	(Chen et al. 2008)
	Crop reside	Methyl violet	Electrostatic interaction, surface precipitation	(Xu et al. 2011)
	Orange peel	Napthalene	Adsorption and partition	(Chen et al. 2011)
	Peanut shell	Trichloroethylene	Adsorption	(Ahmad et al. 2012)

Adapted from (Ahmad et al. 2014; Beesley et al. 2011)

Unlike their organic counterparts, inorganic contaminants are non-biodegradable in the environment. They can be highly toxic to soil biota and any flora or fauna that come into contact with them (Ahmad et al. 2014; Beesley et al. 2011). Inorganic contaminants, especially metals in the environment, generally stem from anthropogenic sources—including mining waste, agricultural runoff, and industrial wastes. Where organic contaminants rely on the high surface and microporosity of biochars for adsorption, the predominant mechanisms in adsorption inorganic contaminants involve ion-exchange, electrostatic attraction, and precipitation (Ahmad et al. 2014). Through complexation

reactions, many types of biochars can capture or immobilize heavy metals and reduce their bioavailability in soils, or remove them from water or leachate (Beesley et al. 2011). Carboxyl groups (-COOH and –OH) contained on the biochars can allow metal cations to form surface complexes on the material and effectively remove the metals from solution (Tong et al. 2011). In soils, biochar application can reduce metal mobility by raising the pH of the soil, decreasing the solubility of the metal. However, in some cases, biochar application to soil mobilized contaminants due to an increased pH and other factors influencing the solubility of the contaminant (Beesley et al. 2010). Table 2.4 illustrates the effects of biochars used for the soil and water remediation of inorganic contaminants.

Table 2.4: Biochars used to remediate inorganic contaminants in soils and water

Media	*Biochar*	*Contaminant*	*Results*	*Source*
Soil	Hardwood, mixed with soil	As, Cd, Cu, Pb, Zn	Increased mobility of As, Cu, Pb mobility	(Beesley and Dickinson 2010)
	Orchard prune residue	Mine tailings with Cd, Cr, Cu, Ni, Pb, and Zn	Reduced leachable Cd, Pb, and Cr. Reduced bioavailability of Cd, Pb, Zn	(Fellet et al. 2011)
	Eucalyptus saligna activated biochar	As, Cd, Cu, Pb, Zn	Increase in extractable As, Zn. Decrease in Pb. Decrease in As, Cd, Cu, Pb in plants	(Namgay et al. 2010)
	Chicken manure	Cd, Cu, Pb	Immobilization of metals	(Park et al. 2011)
Water	Sugar beet tailing	Cr	Electrostatic interaction, complexation, reduction of Cr(VI) to Cr (III)	(Dong et al. 2011)
	Crop straw	Cu	Adsorption from surface complexation	(Tong et al. 2011)
	Cu, Cd, Ni, Zn	Corn straw	Adsorption onto inorganic fraction	(Lima et al. 2010)
	Hg	Soybean stalk	Precipitation, complexation, and reduction of Hg ion	(Kong et al. 2011)

Adapted from (Ahmad et al. 2014; Beesley et al. 2011)

Along with heavy metals, nutrients, especially P in excess or entering source waters can be an inorganic contaminant. Relatively little research has been conducted on the P adsorption capabilities of either unmodified or engineered biochars (Yao et al. 2013b). P adsorbed onto biochars could be reapplied to fields, reducing the overall need for agriculture application. Engineered biochars produced from simple treatment processes have the potential to increase the adsorption capacities of P onto biochars, through increased SA and microporosity from chemical or physical activation, or from tailoring biochars to have greater interactions with negative P ions, such as phosphates contained in agricultural runoff. Metal ions integrated into the surface structure of a biochar could create a positive surface charge, creating electrostatic interactions between the biochar surface and phosphates, and create complexes that would effectively remove P from water.

3 PROPOSED SOLUTION

Reducing the amount of phosphorus contained in agricultural runoff would limit the amount of nutrients entering surface water systems. A reduction in phosphorus where the nutrient is the limiting factor in harmful algal blooms would reduce the size and frequency of harmful algal blooms. Biochars are a promising material that can remove phosphorus from agricultural runoff. With their simplistic production process, inexpensive source material, and physical and chemical characteristic similarities to activated carbons, engineered biochars tailored to remove nutrients from solution could help to control harmful algal blooms.

This study seeks to utilize waste materials commonly found in the area, and through minor modifications during the biochar production process, produce a biochar that is capable of effectively removing phosphorus from an aqueous solution and adsorbing it to the biochar. A biochar that is highly effective as a phosphorus adsorbent has the potential for reapplication as a fertilizer to agricultural fields, limiting the amount of phosphorus lost to surface water runoff in agricultural fields and reducing phosphorus availability in surface waters contributing to harmful algal blooms. Materials obtained do not represent an all-encompassing analysis of locally available materials, but provide an analysis of several biochar production methods with two locally available materials, corn-stalk residue and oak sawdust, obtained at minimal cost.

4 MATERIALS AND METHODS

Three types of engineered biochars were produced from cornstalk residue and sawdust source materials. The material was pyrolyzed after being pretreated with an acid rinse (SA and CA), loaded with a magnesium salt (SMgO and CMgO), or unmodified prior to pyrolysis (SP and CP). Biochars produced were tested and characterized for phosphate adsorption using batch reactor experiments. Materials that removed phosphates from solution were characterized using Langmuir and Freundlich isotherm models.

4.1 RAW MATERIALS

4.1.1 Cornstalk residue

Cornstalk residue was obtained from a local farm in Spencerville, Ohio. The residue was comprised of components of corn that were not used for food or other purposes, including corn stalks, cobs, leaves, and other organic matter treated as waste in an agricultural field (Figure 4.1). The material was broken down into smaller pieces, approximately ¼" to 1" in length with varying widths (Figure 4.2). The cornstalk was not sieved prior to biochar production to simulate an agricultural setting in which material would be roughly broken down, pretreated, and processed in a large-scale pyrolysis reactor.

Figure 4.1: Sample of cornstalk residue, as received

4.1.2 Oak sawdust

Sawdust was provided from Ogonek Custom Hardwoods in Akron, Ohio. The material primarily consists of chainsaw shavings obtained from a single Red Oak tree processed by the company. The material is thin and fibrous, ranging in size from approximately ½" to 3" in length and 1/8" to ¼" wide (Figure 4.2). The oak sawdust was not processed or sieved prior to biochar production for reasons similar to the cornstalk residue preparation.

Figure 4.2: Prepared sawdust (left) and cornstalk residue (right) before pyrolysis

4.1.3 Biochar pre-treatment

Sawdust and cornstalk residue had three conditions prior to biochar production. Biochars produced were unmodified (pristine), acid-rinsed, and magnesium oxide-loaded sawdust and cornstalk biochars (SP and CP, SA and CA, and SMgO and CMgO, respectively (Table 4.1).

Table 4.1: Abbreviations for engineered biochars

	Pre-pyrolysis condition		
Source material	*Unmodified*	*Acid rinsed*	*Magnesium loaded*
Cornstalk residue	CP	CA	SMgO
Sawdust	SP	SA	CMgO

Unmodified biochars (SP and CP) were prepared by rinsing raw materials with reverse-osmosis (RO) water for 90 seconds to remove particulate matter and physical surface contaminants on the materials. After the RO water rinse, SP and CP were oven-dried overnight at 110°C, and stored for a period of up to 2 weeks in closed glass jars prior to pyrolysis.

An acid rinse pretreatment was used to produce the acid-rinsed biochars (CA and SA). The acid rinse pretreatment was accomplished by placing 35.0 g of raw material into an acid bath solution prepared by diluting 100mL of 5.0 M HCl (Fisher) with 900mL of RO water. The materials were placed in the acid bath solution for 60 minutes and manually agitated using a glass stir rod for 60 seconds every 10 minutes (Figure 4.3). To stop acid interactions with the raw materials, material was rinsed with RO water after the acid treatment and oven-dried overnight at 110°C. SA and CA were stored for up to 3 weeks in covered glass jars prior to pyrolysis trials.

Figure 4.3: Cornstalk acid rinse with manual agitation

Magnesium oxide biochars (SMgO and CMgO) were prepared by loading a magnesium salt onto the surface of the raw material. The magnesium salt was loaded onto raw materials by placing 10.0g of each raw material into 200mL of an MgCl solution prepared by dissolving 80.0 g of Fischer $MgCl_2*6H_2O$ salt in 200 mL of RO water. The raw material and solution mixture was mixed at 75 rpm with a SI-300R orbital shaker for a period of 2 hours (figure 4.4). The Mg-loaded raw materials were not rinsed with RO water to prevent the Mg loaded onto the surface of the materials from rinsing off. Mg-loaded sawdust and cornstalk residue was oven-dried overnight and stored in sealed glass jars for a period of 2 days prior to pyrolysis trials.

Figure 4.4: Loading cornstalk residue with MgCl salt using SI-300R orbital shaker

4.2 EXPERIMENTAL METHODS

4.2.1 Pyrolysis trials

Raw materials were pyrolyzed after pretreatment. Pyrolysis was conducted in a 2" diameter steel reactor (Figure 4.5). Material was placed into the reactor, and the reactor was flushed with nitrogen gas for 15 minutes at a flowrate of 2 L/min to remove oxygen contained within the reactor. Nitrogen flow was continued, and the reactor was heated up in a Lindberg furnace to 500°C. The maximum temperature was sustained for an additional 30 minutes after reaching the temperature for a total time active heating of 60 minutes. After shutting off power to the oven, nitrogen flow was sustained for an additional 15 minutes to ensure any remaining heat-based reactions happened under low oxygen conditions. Material was cooled to room temperature and ground up to fine particles (Figure 4.6) using a Coffeemate blade grinder. Samples of prepared biochar were stored in opaque jars for future adsorption testing. A detailed schematic of the pyrolysis apparatus setup can be found in the Appendices, Section 8.4.

Figure 4.5: Steel reactor for pyrolysis trials

Figure 4.6a: Sawdust before pyrolysis, after pyrolysis, and after final production steps

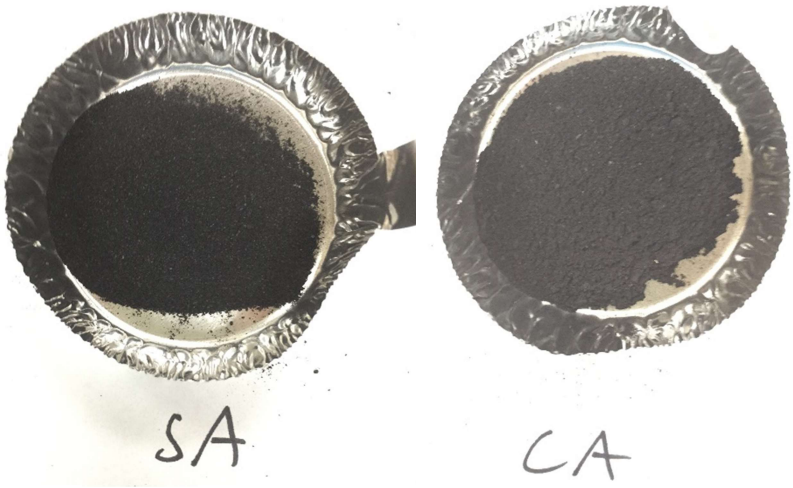

Figure 4.6b: Enlarged image of final biochar products.
Acid-rinsed sawdust (left) and Acid-rinsed Cornstalk (right)

4.2.2 Phosphorus adsorption and desorption

4.2.2.1 Standards and evaluation methods

A stock solution of 1g/L PO_4^{3-} was prepared by dissolving 1.453g of Fischer sodium phosphate monohydrate, $NaH_2PO_4*H_2O$ in 1.0 L of RO water. Appropriate dilutions, from 30 mg/L to 300 mg/L PO_4^{3-} solution were prepared in RO water.

Phosphate adsorption/desorption was evaluated in batch reactor experiments. For P-sorption trials, 40mL of varying concentrations of PO_4^{3-} solution was placed in 50mL Fisher Falcon tubes with varying masses of prepared biochar (Figure 4.7). Reactions took place in a Big SHOT III hybridization oven (Figure 4.8) at a 30°C isotherm and a rotational speed of 60 spm. Samples were filtered through 0.20 µm filters to remove biochar from PO_4^{3-} solutions and prevent interference with PO_4^{3-} concentration measurements.

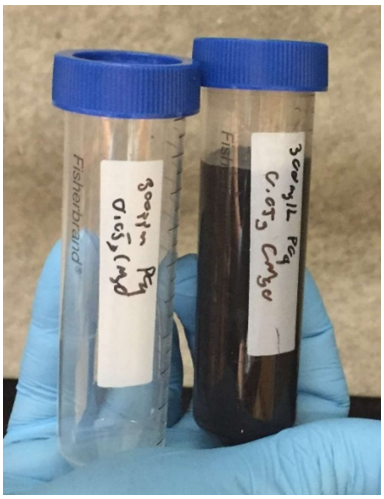

Figure 4.7: 50 mL Fisher Falcon tube, empty and with 40mL of 30 mg/L PO_4^{3-} Solution and 0.1 g CMgO

Figure 4.8: Big SHOT hybridization oven used for adsorption isotherm experiments

Phosphate concentrations of solution were testing using a Hach DR/890 Colorimeter and Hach Method 8048 for Orthophosphate 0.2 to 2.50mg/L PO_4^{3-}, concurrent with USEPA PhosVer 3 (Ascorbic Acid) Method (Hach). To test all concentrations (0-300 ppm PO4), appropriate sample dilutions were required to be within the range of the Hach testing method, and back calculated to their actual concentration.

4.2.2.2 RO controls

A negative control test was conducted through testing the release of PO_4^{3-} from biochars. Batch reactor tests of biochar-RO water were prepared in duplicate with 100 mg of biochar placed into 40 mL of RO water. PO_4^{3-} concentration was measured after a period of 24 hours to determine amount of PO_4^{3-} leaching into water from prepared biochars. Two PO_4^{3-} concentration samples were taken for each batch reactor (See Experimental Matrix in Appendix Section 8.3).

4.2.2.3 Phosphorus adsorption

Initial time to reach equilibrium was determined using an approximate 30mg/L (ppm) PO_4^{3-} solution and SP. Batch-reactor experiments were run in triplicate with 5 mL of 20g/L SP slurry placed into 40mL of 30mg/L PO_4^{3-} solution. P-adsorption reaction trials took place in the hybridization oven for a period of 24 hours, 72 hours, and one week. Initial and final PO4 concentrations were measured, and results compared to determine if any significant change occurred from 24 hours to 72 hours and one week. From these trials, equilibrium time was determined and used for further testing.

An initial screening test for phosphate adsorption capacity was conducted with 100mg of each biochar placed into 40 mL of 30 ppm PO_4^{3-} solution. Batch-reactors were run in triplicate for 24 hours, with initial and final PO_4^{3-} concentrations measured. Two PO4 samples were taken from each batch reactor to account for variability. Initial and final

24-hour concentrations were used to create a normalized equilibrium graph, shown in the results section.

SMgO and CMgO, materials that displayed high PO_4^{3-} removal, were further evaluated, with ranges of 10 to 100 mg biochar placed into 30 to 300 ppm PO_4^{3-} solution. Batch reactors were run in triplicate for a period of 24 hours, with initial and final PO_4^{3-} concentrations measured. Two PO_4^{3-} samples were taken from each batch reactor to account for variability.

4.3 ANALYTICAL METHODS

The mass of biochar was measured throughout the production process. The percent yield of biochar from pyrolysis can be characterized by Equation 4-1.

(Eq 4-1) $$y = \frac{M}{Mi} * 100$$ Biochar yield

Where y= biochar product yield, %
Mi = initial mass of source material, g
M = final mass of pyrolyzed biochar, g

The bulk density of raw materials and density of engineered biochars (Equation 4-2) of was calculated by measuring the mass of uncompacted material required to fill a specific volume in a graduated cylinder.

(Eq 4-2) $$\rho = \frac{m}{V}$$ Bulk density

Where ρ = density (bulk or apparent), g/L
m = mass of material, g
V = volume of uncompacted material, L

Adsorption characteristics of the engineered biochars were calculated during the 30 mg/L phosphate adsorption screening test and throughout the magnesium oxide biochar adsorption tests. The removal efficiency (Eq 4-3) was only calculated for the 30 mg/L phosphate adsorption screening test.

(Eq 4-3) $$e = \frac{C_{eq}}{Ci} * 100$$ Adsorption efficiency

Where e = PO_4^{3-} removal efficiency of engineered biochars, %
Ci = initial PO_4^{3-} concentration, mg/L
C_{eq} = final PO_4^{3-} concentration, mg/L

The adsorption capacity of biochars was found using Equation 4-4, and applied to both a Langmuir (Eq 4-5) and Freundlich (Eq 4-6) isotherm models to characterize the adsorption properties of magnesium oxide biochars. A linearized form of the Langmuir isotherm model (Eq 4-7) was fitted to a data plotted on a logarithmic C_A (x-axis) to q (y-axis) graph to determine the Langmuir adsorption parameters n and K. The linearized

Freundlich isotherm model (Eq 4-8) was curve-fitted to a C_{eq} (x-axis) vs C_{eq} /q (y-axis) graph to determine the b_A and Q_m Langmuir isotherm constants.

(Eq 4-4) $$q = \frac{V}{M}(C_i - C_{eq})$$ Adsorption capacity

Where q = adsorption capacity, mg adsorbate / g adsorbent
V = volume of aqueous solution, mg/L
M = mass of adsorbent, g

(Eq 4-5) $$q = \frac{Q_m b_A C_{eq}}{1 + b_A C_{eq}}$$ Langmuir isotherm model

Where Q_m = max adsorbent phase concentration of adsorbate (mg adsorbate / g adsorbent)
b_A = Langmuir adsorption constant (L/mg)

(Eq 4-6) $$q = K C_{eq}^{\ 1/n}$$ Freundlich isotherm model

Where K = Freundlich adsorption capacity parameter
1/n = Freundlich adsorption intensity parameter

(Eq 4-7) $$\frac{C_{eq}}{q} = \frac{1}{b_A Q_M} + \frac{C_{eq}}{Q_M}$$ Linearized Langmuir model

(Eq 4-8) $$log\ q_A = log K_A + \left(\frac{1}{n}\right) log C_{eq}$$ Linearized Freundlich model

Sample calculations from data gathered in the experiment can be found in the Appendices, Section 8.4.

5 RESULTS AND DISCUSSION

5.1 PYROLYSIS YIELDS

Source materials produced a solid biochar, synthesis gas (syngas) and an oily liquid known as bio-oil during slow pyrolysis. As shown in Figure 1, unmodified sawdust (SP) yielded 24.1% and cornstalk residue (CP) yielded a slightly higher 33.9 %, by mass, of solid biochar after pyrolysis of the source material. Acid-rinsed biochars displayed a slight increase in mass retention when compared to the unmodified biochars. The pyrolysis of acid-rinsed cornstalk residue (CA) yielded 32.6 % biochar; a decrease of 1.3% compared to CP. Acid-rinsed sawdust (SA) yielded 27.8% biochar, a 3.6% increase. The magnesium-loaded biochars yielded much more solid compared to the source material, with magnesium-oxide cornstalk biochar (CMgO) yielding 71.6% and MgO-sawdust biochar (SMgO) yielding 91.0 % of the source material used.

Syngas and bio-oil production were observed qualitatively throughout the pyrolysis trials. The production of syngas was noted as a smoke with an odor not unlike the smoke produced during the combustion of similar raw materials. Syngas was produced approximately 10 minutes into heat application and ending 15 minutes after the heating portion of the pyrolysis trials. Bio-oil produced during pyrolysis built up in the exhaust tubes, restricting airflow several times throughout all of the trials. To account for bio-oil production, a larger diameter exhaust tube was used later in the experiment.

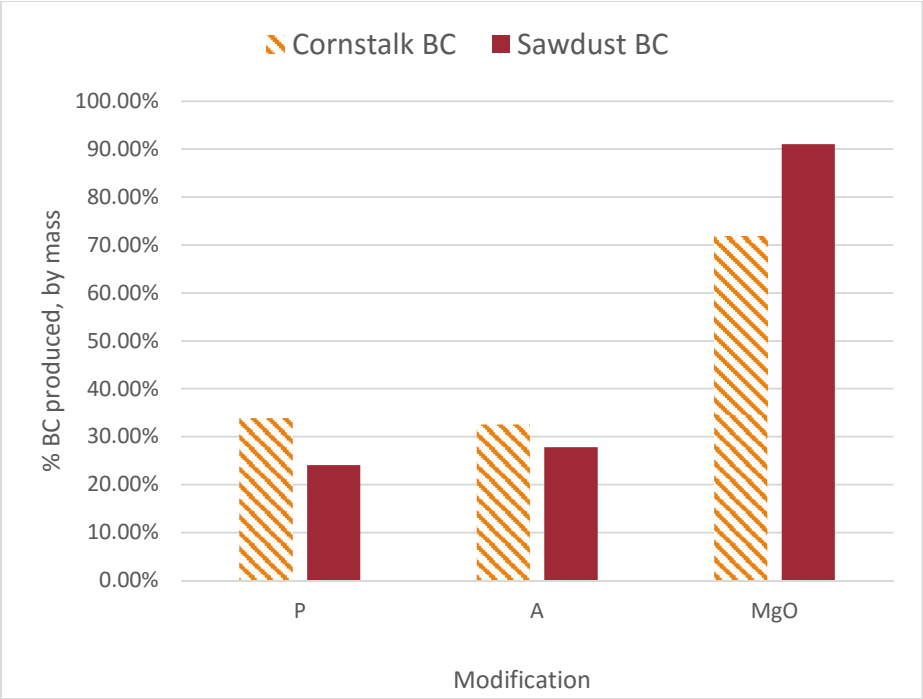

Figure 5.1: Biochar yield by mass for different engineered biochars
P = pristine (unmodified), A = acid-rinsed, MgO = magnesium oxide biochars

Typical slow-pyrolysis trials yield between 20-40% by mass of solid material for both wood-based biochars and corn stalk biochars (Guo and Bi 2015) (Table 2.2, in literature review). The experiment yielded results within those ranges for both acid-rinsed and as-received materials (Figure 5.1), with corn-based biochar yielding 30-35% by mass and wood-based biochar with slightly lower yields between 24% and 28%. Any variation in the biochar yield could have resulted from non-ideal reactor conditions. The heating and cooling rates of the pyrolysis reaction were not controlled, and the reactor was not ideally packed or insulated, observed in a heat gradient ranging from 490°C to 530+ °C. In addition, the reactor may not have achieved truly low-oxygen conditions, as no instruments were available to monitor the gas composition after piping in nitrogen gas for 15 minutes. Higher oxygen content in the reactor would create conditions closer to combustion, which would volatilize more material and produce more unfavorable materials such as ash or syngas. A higher degree of control on the pyrolysis reaction could potentially increase reliability of biochar production and the amount of solid material yielded per reactor run, as the temperature and heating gradient are two major factors that control biochar characteristics (See section 2.2.2, Biochar production).

Both the SMgO and CMgO biochars had an uncharacteristically high production efficiency. This is in part due to the Mg salt pretreatment that loaded Mg onto the biochar prior to pyrolysis. The extra mass added from Magnesium being deposited onto the surface of the biochar was not accounted for. To improve the accuracy of solids yield from both MgO biochars, the mass of each material should be recorded post-treatment and pre-pyrolysis to determine the amount of mass lost from both Mg loaded onto the source material and the material itself. Even with obtaining a more accurate mass measurement for the magnesium salt pretreated biochars, the production efficiency is expected to be higher than the other biochars produced. Magnesium salt loaded onto the surface of raw materials would provide extra mass that would not volatilize during pyrolysis. The same amount of material may be converted to syngas and bio-oil, but the raw material has more initial mass. As a result, the yield of MgO biochars should be higher.

Syngas and bio-oil production were observed qualitatively, as measuring their compositions or production efficiencies at specified pyrolysis conditions were outside of the scope of the study. Syngas is typically composed of H_2, CO, O_2, CH_4, CO_2 and C^{2+}, with CO_2, CO, and O_2 gases being the dominant products. Bio-oil produced during the pyrolysis of similar raw materials was found to have a pH of 2.5-4 and an elemental composition of primarily C and O, with smaller fractions of H,N, and S (González et al. 2003; Guo and Bi 2015; Tinwala et al. 2015). Under the slow pyrolysis conditions in this experiment, a syngas yield of 35% and bio-oil yield of 30% could be expected (Lehmann and Joseph 2009; Mohan et al. 2014; Qian et al. 2015; Sohi et al. 2010). To account for bio-oil production in future experiments, the recommendation is to install a collecting

system to collect and characterize the bio-oil produced. Syngas produced in the experiment could be captured and characterized by gas chromatography.

5.2 BIOCHAR CHARACTERIZATION

Several properties of both the raw materials and engineered biochars were used to characterize the biochars. The bulk density of the biochars was calculated and compared to the bulk density of the source materials. The interactions between biochars and water were observed and recorded throughout the experiment. Several visual observations were made on the physical appearance of pyrolyzed materials that could be used to characterize the physical and chemical characteristics of the engineered biochars.

5.2.1 Bulk Density

All of the biochars produced in this experiment increased in density after pyrolysis and processing of pyrolyzed material, shown in figure 5.2. The sawdust-based biochars increased from a raw material bulk density of 29.9 g/L to a biochar bulk density range of 306.6 g/L (SP) to 473.2 g/L (SMgO), an increase between 1,000% -1,500%. In comparison, the cornstalk residue based biochars were less dense and had less of a change in density during pyrolysis. Cornstalk residue biochar showed an approximate 200 % to 350% increase from raw material to biochar, with a raw material bulk density of 81.4 g/L and biochar bulk density ranging from 188.3 g/L (CP) to 285.5 g/L (CMgO).

As can be observed in figure 5.2, both cornstalk residue and sawdust based biochars displayed similar trends in biochar densities. The unmodified biochar was the least dense of the pyrolyzed materials, followed by the acid-rinsed and MgO biochars, the densest. The apparent densities of the acid-rinsed biochars were 10-15% higher, and the apparent densities of the magnesium oxide biochars were 50-60% than the apparent densities of the unmodified biochars.

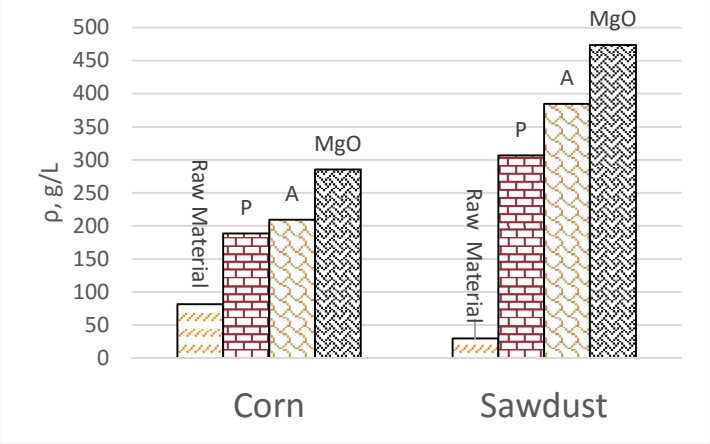

Figure 5.2: Bulk density of prepared biochars vs raw materials
P = pristine (unmodified), A = acid-rinsed, MgO = magnesium oxide biochars

In comparing the corn and sawdust-based biochars, the magnitude difference in density change is likely from volatile matter and the fixed carbon contained within the source materials. Tinwala et al. noted that sawdust biomass had a much higher percent of its mass comprised of volatile matter and fixed carbon in comparison to agricultural feedstocks, which could contain nutrients and a higher percent of inorganics due to fertilizer and soil amendments (Tinwala et al. 2015). As source materials are heated through pyrolysis, volatile matter would vaporize and be removed from solids. A higher percentage of volatile matter would translate into more total mass lost, and a higher density gain from remaining carbonaceous content and inorganic materials. This correlates to a higher percentage of mass lost and apparent density increase of sawdust-based biochars in comparison to cornstalk-based biochars.

The bulk densities of CP and SP biochar were 188 and 307 g/L respectively (Figure 5.2). These values are close to expected values. Huang et al. found a bulk density of approximately 200 g/L for corncob-derived biochar, and 300 g/L for peanut hull and rice hull-derived biochar, which have similar volatile matter and fixed carbon content to sawdust-derived biochar (Huang et al. 2012; Tinwala et al. 2015). The slightly higher densities of the acid-rinsed biochars in comparison to the unmodified biochars could be due to the acid's interaction with surface characteristics of the raw material. Acids can potentially reach the micro and meso pores of the source material structure, exposing more volatiles contained in the raw materials to heat and resulting in a slight increase in density as more of the less-dense volatiles are converted to bio-oil or syngas.

Both MgO biochars showed an approximate 50% increase in apparent densities from unmodified biochar. In previous research with similar pretreatment methods, nano-sized MgO crystalline structures were found through to be integrated into biochar structure (Yao 2013; Yao et al. 2011; Zhang et al. 2012). This formation of an MgO-biochar nanocomposite would increase the apparent density of a biochar as MgO complexes are formed onto the structure, increasing the mass per volume of the pyrolyzed material. The increase in apparent densities observed in these experiments suggest that the selected materials and pretreatment methods successfully created MgO- biochar nanocomposites. Using X-ray diffraction or electron microscopy is recommended to fully verify the formation of Mg-O nanocrystals on the biochar surface.

5.2.2 Interactions with water

The interactions between each engineered biochar and water were observed in preparing P-adsorption experiments. SMgO and CMgO displayed hydrophobic characteristics, repelling water (Figure 5.3a) and settling quickly in solution (Figure 5.4a). In comparison, CA, SA, CP, and SP were more hydrophilic. These biochars mixed well with water and stayed suspended in solution for much longer than the MgO biochars (Figure 5.4b). An oily film with some surface tension (Figure 5.3b) was observed when the acid-

rinsed and unmodified biochars were being used to prepare biochar slurries for adsorption experiments.

Biochar surfaces produced from low temperature pyrolysis tend to be hydrophobic (Sohi et al. 2010). While the MgO biochars displayed this characteristic, the other engineered biochars did not. The suspension in an aqueous solution of the unmodified and acid-rinsed biochars could be due to negatively charged carboxyl groups, and a general negative surface charge that is typical of biochars (Ahmad et al. 2014). The oily surface created from the unmodified and acid-rinsed biochars could come from lignin, found in many organic materials. In comparison to cellulose and hemicellulose found in organic matter, lignin has a lower reactivity (Khezami et al 2005). The lignin found in the raw materials used in these experiments may not decompose or only partially decompose, and allowing the lignin contained in the now pyrolyzed material to interact with water. A quicker settling and hydrophobic biochar would be more suited to adsorption processes, as the material could easily be separated out from an effluent stream.

Figure 5.5a: Hydrophobic CMgO

Figure 5.5b: Hydrophilic CA

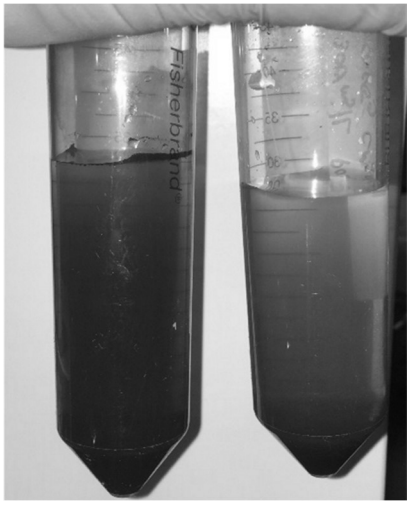

Figure 5.4: SA (left) and SMgO (right), 15 minutes of settling after agitation

5.2.3 Visual characteristics

The sawdust-based biochar was noted to have a black color and had fine-grained particles, suggesting a high level of carbon content in the pyrolyzed material (Figure 5.5a). In comparison, the cornstalk-based biochars had more of a brown color and were coarser, with larger particle sizes (Figure 5.5b). The coloration of the corn-based biochars hints at a lower fixed carbon content and more inorganics and nutrients contained in the material. This is supported by the biochar yields of the different raw materials (Figure 5.1), and explains why the apparent density did not change as much from raw cornstalk residue to biochar compared to raw sawdust to sawdust based biochar (Figure 5.2).

Figure 5.5: Highlighting the color variation in CA (left) and SA (right)

The MgO biochar was observed to have metallic crystals in the pyrolysis product. These metallic particles hint that more MgO was produced than that which could be integrated into the biochar structure, and some of the material did not react to form nanocrystal structures on the MgO biochar. These particulates may affect other results and characteristics of the engineered MgO biochars such as bulk density, P adsorption efficiencies, and surface characteristics.

5.3 PHOSPHATE ADSORPTION RESULTS

5.3.1 Desorption of phosphates

A negative control of RO interference was measured using Hach method 8048, ascorbic acid to determine the amount of background PO_4^{3-} expected from RO water. An average PO_4^{3-} concentration of 0.0475 mg/L was measured and determined to be negligible compared to the range of PO_4^{3-} (30-300 ppm) used during phosphate adsorption experiments. The RO interference is displayed as error bars in the biochar desorption testing (Figure 5.5a).

Before testing the PO_4^{3-} adsorption characteristics of engineered biochars, a negative control test of biochar desorption of PO_4^{3-} into reverse osmosis (RO) water was conducted (Figures 5.6a and 5.6b). MgO and acid-treated biochars of both source materials released small amounts of PO_4^{3-} into RO water (Figure 5.6a), which are below the limits of the testing equipment (0.2 mg/L PO_4^{3-}). Shown in figures 5.6a and b, the unmodified sawdust also released minimal amounts of PO_4^{3-}. The CP biochar released 7.2

g/L PO_4^{3-} into RO water, 50-100 times more than the release measured in all of the other biochars.

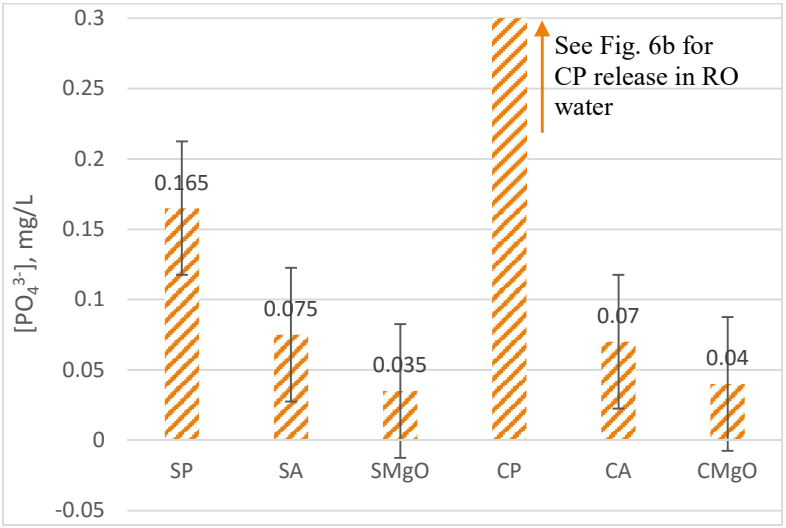

Fig. 5.6a: PO_4^{3-} release in RO water after 24h with RO interference error bars
Note: SP = unmodified sawdust, SA = acid-rinsed sawdust, SMgO = magnesium loaded sawdust CP = unmodified cornstalk, CA = acid-rinsed cornstalk, CMgO = magnesium loaded cornstalk

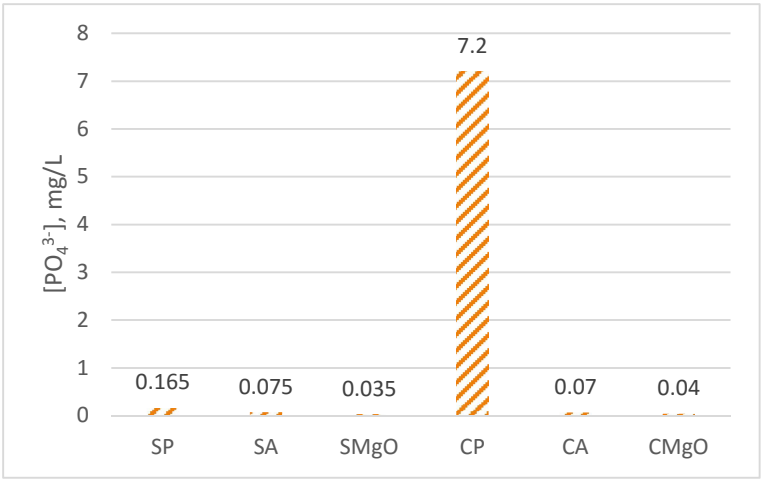

Fig. 5.6b: PO_4^{3-} release in RO water after 24 h, enlarged
Note: SP = unmodified sawdust, SA = acid-rinsed sawdust, SMgO = magnesium loaded sawdust CP = unmodified cornstalk, CA = acid-rinsed cornstalk, CMgO = magnesium loaded cornstalk

None of the engineered biochars in this study, except for CP, are expected to release phosphates into the environment without adsorbing any contaminants or nutrients. Unmodified biochars should not be used as a PO_4^{3-} adsorbent, as they may desorb more nutrients into agricultural runoff than they adsorb. While a release of PO_4^{3-} was expected in the CP biochar due to rendering many of the nutrients in the raw material more bioavailable and open to exposure, the decrease to a negligible PO_4^{3-} release with the acid pretreatment was not expected. This decrease in PO_4^{3-} desorption is likely due to the acid removing nutrients and contaminants contained on the surface and within some of the pore structures of the raw material prior to pyrolysis. To determine the effect both

pretreatment methods (acid rinsed and MgO-loading) have on the structure, surface chemistry, and bioavailability of nutrients within the biochar, further analysis should be conducted.

5.3.2 Phosphate adsorption tests

The unmodified (CP and SP) biochars showed no adsorption capacity for PO_4^{3-} at 30 mg/L. Both materials released phosphates into solution, adding an additional 7.2 % or 22.4 % of phosphates to the 30 ppm solution (Table 5.1, Figure 5.7). The acid-rinsed biochars shifted towards positive adsorption characteristics, with the SA biochar adding 2.3% more PO_4^{3-} compared to the 7.2% release of SP, and the CA biochar adsorbed 13.5% of PO_4^{3-} in the 30 ppm PO_4^{3-} solution, compared to the 22.4 % increase from CP.

Table 5.1: Removal efficiencies and q values at 30 ppm PO_4^{3-}

Material	*% removal*	*q, mg adsorbate/g adsorbent*
SP	-7.17%	-1.10
SA	-2.32%	-3.41
SMgO	99.35%	12.58
CP	-22.39%	-2.84
CA	13.49%	1.71
CMgO	98.88%	12.52

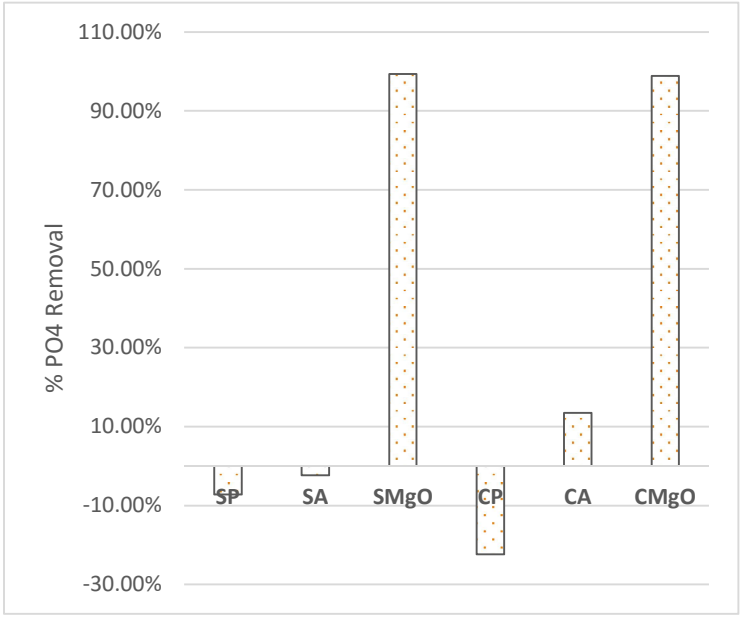

Figure 5.7: Removal efficiencies of biochars at 30 ppm PO_4^{3-}
Note: SP = unmodified sawdust, SA = acid-rinsed sawdust, SMgO = magnesium loaded sawdust CP = unmodified cornstalk, CA = acid-rinsed cornstalk, CMgO = magnesium loaded cornstalk

Shown in Table 5.1 and Figure 5.7, both MgO biochars showed ~99% removal at 30 ppm PO_4^{3-}. SMgO showed slightly higher adsorption capacities (q) than the CMgO, with 12.6 and 12.5 mg PO_4^{3-} / g biochar respectively. Both MgO engineered biochars showed increased q values as the ratio of adsorbate to adsorbent increased, with the q of SMgO becoming increasingly larger as the ratio increased (Figure 5.8). When varying the mass of biochar used in a 30 ppm PO_4^{3-} solution from 0.1g to 0.01 g, CMgO displayed an adsorption capacity range of 12.5-39.7 mg PO_4^{3-} / g biochar and SMgO had a range of 12.6-56.9 mg PO_4^{3-} / g biochar.

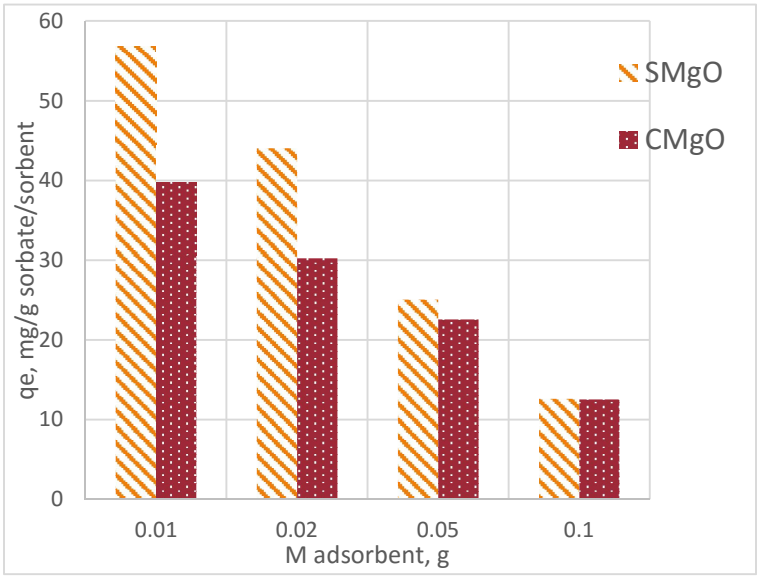

Figure 5.8: 30 mg/L PO_4^{3-} adsorption capacity with variable mass SMgO and CMgO
SMgO = magnesium loaded sawdust biochar, CMgO = magnesium loaded cornstalk residue biochar

SMgO displayed a higher adsorption capacity than CMgO with most of the concentrations tested in this experiment (Figure 5.9). At lower concentrations (30-150 ppm PO_4^{3-}), SMgO had a higher q, ranging from 12.6-101.7 mg PO_4^{3-} / g biochar, compared to the q of CMgO, ranging from 12.5-60.6 mg PO_4^{3-} / g biochar. Using 300 ppm PO_4^{3-} and 0.05 g of biochar, the CMgO displayed a much higher q with a maximum value of 249.6 mg PO_4^{3-} / g biochar compared to SMgO's maximum q of 174 mg PO_4^{3-}/g biochar.

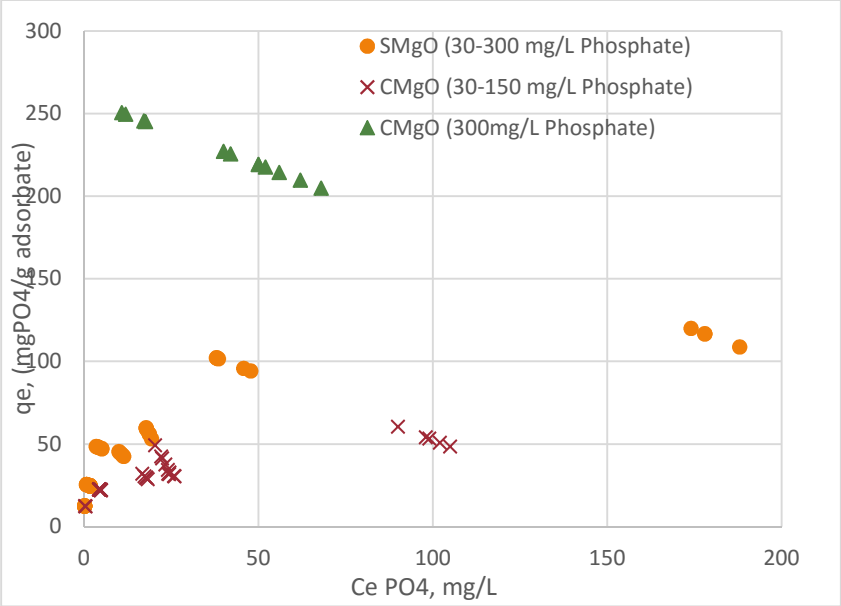

Figure 5.9: Ce vs qe of CMgO and SMgO

SMgO = magnesium loaded sawdust biochar, CMgO = magnesium loaded cornstalk residue biochar

As shown in figures 5.10a and 5.10b, The MgO biochars were characterized using linearized Freundlich and the associative Langmuir isotherm models. For Freundlich constants determined from a linear curve fit to a logCe vs logq plot (Fig. 5.10a), the sawdust based MgO biochar had an n value of 2.94, k value of 23.22, and an R^2 value of 0.94. The CMgO had an n value of 2.41, k value of 16.13, and an R^2 value of 0.44.

The associative Langmuir isotherm model (Figure 5.10b) showed slightly higher correlations between data points and the linear curve fit of a Ce vs Ce/Qe plot. The linear curve fitted to results showed R^2 values of 0.98 for SMgO and 0.63 for CMgO. The SMgO linear curve fit showed a Q_m value of 119.05 and b_A of 0.11. The CMgO linear curve fit results were a Q_m value of 70.42 and b_A of 0.15. A summary of both isotherm models can be found in Table 5.2. Equations 4-4 through 4-8 in section 4.3 of materials and methods section of this thesis detail the isotherm models and constants used.

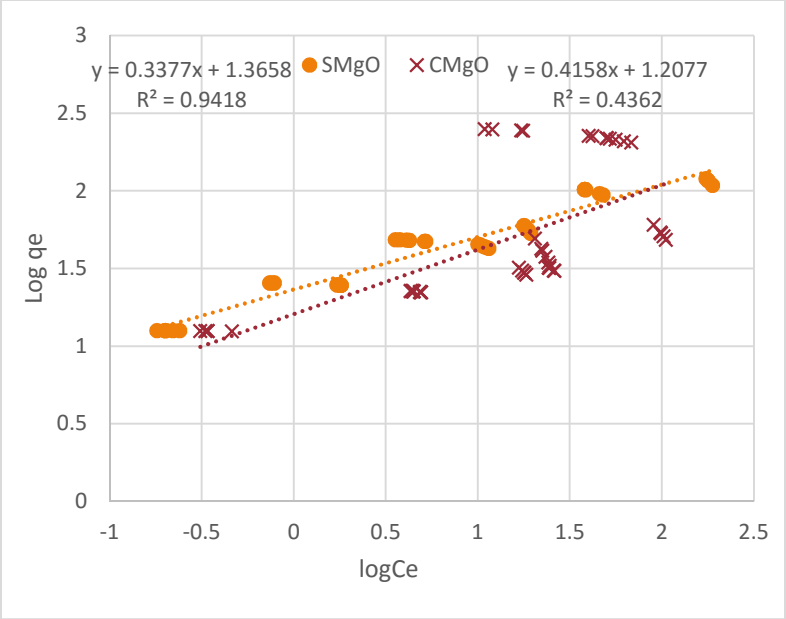

Figure 5.10a: Linearized Freundlich isotherm model of SMgO and CMgO

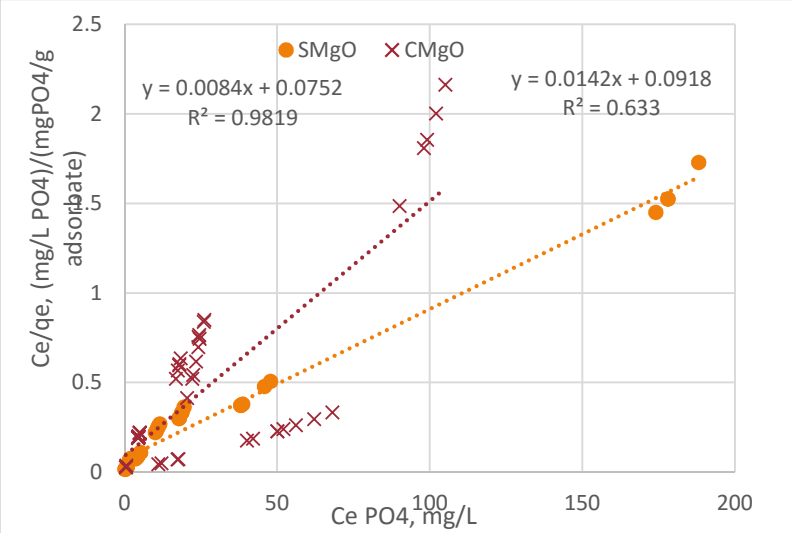

Figure 5.10b: Linearized Associative Langmuir isotherm model of SMgO and CMgO
SMgO = magnesium loaded sawdust biochar, CMgO = magnesium loaded cornstalk residue biochar

Table 5.2: Isotherm model constants[1]

	Langmuir			Freundlich		
Biochar	Q_m	b_A	R^2	n	k	R^2
SMgO[2]	119.05	0.11	0.98	2.94	23.22	0.94
CMgO[2]	70.42	0.15	0.63	2.41	16.13	0.44

Notes: 1- For derivation of isotherm linear models and constants, see section 4.3, analytical methods, in materials and methods section
2- SMgO = magnesium loaded sawdust biochar, CMgO = magnesium loaded cornstalk residue biochar

5.4 ADSORPTION MECHANISMS AND BIOCHAR CHARACTERISTICS

5.4.1 Surface area and porosity

Much like activated carbons, biochars typically have a much higher surface area and pore volume than their source material, which make them superior adsorbents to their raw materials(Ahmad et al. 2014; Anawar et al. 2015; Huang et al. 2012; Lehmann and Joseph 2009). Sun et al (2015) found that adding acids to activate biochar s generally decreased their surface area (Table 5.3) and total pore volume. The stronger acids either collapsed or blocked a portion of the micropores, which resulted in a decrease in surface area, total pore volume, and average pore width. However, the acid treatment method greatly increased the adsorption capacities of methyl blue, an organic contaminant. As the acid used in this experiment is of comparable strength, similar changes could have occurred.

Highlighted in Figure 5.6 and Table 5.1, the adsorption characteristics of the acid-rinsed biochars changed slightly, which suggests a change in the surface structure of the acid-rinsed biochars. Since surface area and porosity are not major mechanisms for the adsorption of inorganic contaminants such as phosphates, little change in adsorption capacity was expected. Complexation is possibly the major adsorption mechanism, which is discussed in section 5.4.2 on the following page. SA was measured to release a small amount of PO_4^{3-} into solution, while CA showed slight adsorption capabilities. This adsorption capacity was unexpected as the unmodified corn-based biochar released much higher amounts of PO_4^{3-} in comparison to the unmodified sawdust-based biochar. The acid rinse pretreatment method may have increased or decreased the physical surface characteristics of CA and SA, but may have removed surface nutrients that would otherwise be released into solution.

Using the CO_2 adsorption method and transmission electron microscopy (TEM) image analysis, MgO biochars were found to have a much higher surface area compared to all other biochars observed, and were dominated by micropore structures with an average pore width of 1.5nm or less (Table 5.3) (Yao et al. 2013b; Zhang et al. 2012). This superior surface area and microporosity of MgO biochars nanocomposites suggests that the material would provide for an effective adsorbent in water and soils. The MgO biochar engineered in this experiment had similar production parameters with different source materials. As a result, the surface area, total pore volume, and pore structure should be similar, with some variations depending on the material used. To verify the pore structures of engineered biochars, methods such as TEM imagery are recommended. To determine the total surface area of the biochars in this experiment, the BET CO_2 adsorption method is recommended.

Table 5.3: Surface area and pore characteristics of previous biochar studies

Raw Material	*Pretreatment Method*	*Surface Area (m^2/g)*	*Analysis Method*	*Pore Characteristics*	*Source*
Peanut hull	N/A	2.53	BET (N2 gas assumed)(1)	Average pore width 31.38 nm	Huang et al 2012
Corncob	N/A	3.32	BET (N2 gas assumed)(1)	Average pore width 22.05 nm	
Eucalyptus sawdust	N/A	1.57	BET (N2 adsorption)	Average pore width 7.45 nm	Sun et al 2015
Eucalyptus sawdust	Acid	0.69-1.28	BET (N2 adsorption)	Average pore width 5.87-14.34 nm(2)	
Pine wood	MgO	18.9	BET (N2 adsorption)(3)	Dominated by micropores (<1.5 nm)	Zhang et al, 2012
Peanut Shells	MgO	2.8	BET (N2 adsorption)(3)	Dominated by micropores (<1.5 nm)	

Notes: (1) -BET method was stated, but the gas used was not included in the methods. N2 is assumed, as similar values are found in other studies
(2) - Citric acid, the strongest acid in the study, was found to increase pore width. Acetic acid and tartaric acid both decreased avg. pore width
(3) - N_2 adsorption is not effective at determining total surface area when the surface structure of the biochar is dominated by micropores (<1.5nm). CO2 adsorption found a surface area of 432.6 m^2/g and 346.5 m^2/g for pine wood and peanut shell-based biochars respectively

5.4.2 Adsorption characteristics of MgO biochars

The high adsorption capacity of the MgO biochars can be attributed to several factors. Rather than block micropores for adsorption sites, MgO nanocrystals enhance the adsorption capabilities of the engineered biochar. Surface area and pore volume analyses conducted in previous research showed that MgO- biochar display high surface areas dominated by micropores (Table 5.3), characteristics observed in effective activated carbons. Electrostatic interactions between the phosphate anion and Mg-O cation bring the nutrient close to the surface of the biochar. Yao et al (2013) documented a complexation reaction occurring on the biochar surface between the MgO and PO_4^{3-}. Phosphate precipitated from solution and deposited onto the biochar, forming magnesium-phosphate complexes ($MgHPO_4$ and $Mg(H_2PO_4)_2$) on the surface. Similar conditions during the experiments are expected, but further analysis should be conducted on biochar - phosphate interactions with the engineered MgO biochars to verify this occurrence with the experimental setup in this thesis.

The superior adsorption capacities of the sawdust-based MgO biochar at lower concentrations is likely in part due to the source material compositions. With a higher nutrient and mineral content, the surface of CMgO could interact with the inorganics already contained in the material (such as phosphates, nitrates, or clay minerals). MgO-

nutrient interactions could block micropores with a larger chemical structure or block active adsorption sites that could be utilized in PO_4^{3-} adsorption.

SMgO displayed a high R^2 value in both the Freundlich and Langmuir adsorption models (Figures 5.9a and 5.9b, Table 5.2), which hints that the sawdust-based biochar can be characterized by these typical isotherm adsorption models. The R^2 value was higher in the Langmuir associative isotherm model, which suggests that physisorption through a linear monolayer adsorption is the major mechanism through which the SMgO biochar interacts with PO_4^{3-} in water. To further verify this model, an extended range of adsorbate to adsorbent ratios should be tested.

CMgO biochar did not match either the associative Langmuir or Freundlich isotherm models particularly well (Figure 5.9a and 5.9b), showing R^2 values of 0.44 and 0.63 respectively (Table 5.2). Langmuir and Freundlich isotherms describe physisorption, so little correlation between these may suggest that chemisorption contributes to the adsorption characteristics of the cornstalk-based biochar. In addition, the composition of the biochar source material is expected to play a major role in the change in adsorption mechanisms, as cornstalk residue will typically have more inorganics (including nutrients) and organics within the raw material's structure. These extra materials in the cornstalk residue structure may interact with the MgO nanocrystals formed on the biochar structure. Other models may provide a better fit for the CMgO, but more research is needed on the adsorption mechanisms and characteristics of the engineered biochar before any conclusions can be made.

5.5 PRACTICAL APPLICATIONS

5.5.1 Biochar Production

To scale up to production scale of biochars, a continuous-feed reactor such as the continuous multiple hearth kiln (Figure 5.11) would provide for a quick and efficient method of producing biochars. Typical kilns used for charcoal production are capable of producing 2.5 tons of charcoal/hour, and offer a superior control of reaction properties (Lehmann and Joseph 2009). The kiln below could be easily adapted to flow N_2 or another inert gas to promote pyrolysis, and provide a heating gradient throughout the reactor to control the heating rate and final temperature of biochar production. A contaminant management system such as air stripping or gas adsorption would help mitigate the syngas produced during production.

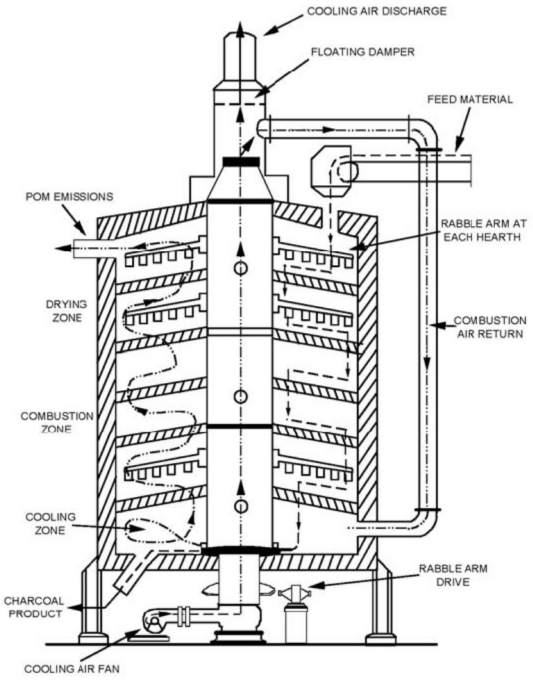

Figure 5.11: Multiple hearth kiln
Source: EPA (1995)

Before the development of petroleum-based products, kilns were used to produce bio-oil for fuel (Lehmann and Joseph 2009). If typical yields of bio-oil from the multiple-hearth kiln were condensed and collected into one place, the bio-oil produced from pyrolysis could be captured and used as fuel for the kiln, saving on external energy usage and removing a potential waste stream from biochar production.

5.5.2 Potential biochar applications

Although unmodified corn-based biochar would not be an efficient P adsorbent for nutrient runoff management, desorption of phosphates into RO water suggests that the engineered biochar has potential as a soil amendment to increase crop growth. Various studies have shown that biochar soil amendments can significantly increase crop growth and fertility through various mechanisms. (Atkinson et al. 2010; Biederman and Stanley Harpole 2013; Kookana et al. 2011; Krishnan and Haridas 2008; Qian et al. 2015; Sohi et al. 2010). The ease at which phosphates desorb from the CP biochar could additionally increase the soil fertility and reduce the overall need for fertilizer application, reducing the amount of nutrients contained in agricultural runoff.

The high adsorption of MgO biochars indicates that these biochars would be an effective P adsorbent to control PO_4^{3-} contained in agricultural runoff. To fully test the potential for PO_4^{3-} removal, a mixture of typical agricultural runoff constituents should be used for future PO_4^{3-} adsorption tests, as other inorganic or organic contaminants could interfere with P adsorption characteristics.

In addition, PO_4^{3-} -laden biochars with a high adsorption capacity have a P content (approximately 20% Phosphate with a q of 250 mg phosphate/g biochar) comparable to or higher than commercial agricultural fertilizers (Smart Fertilizer 2016). If an applicable desorption technique was developed for P-laden biochars, the MgO biochars engineered in this experiment could be efficient fertilizers or agricultural soil amendments. Previous research indicates that P-laden biochar acted as a slow-release fertilizer, releasing P into aqueous solution multiple times and mimicking a typical slow release nutrient source for plant uptake (Yao et al. 2013a). Using P-laden biochars as a slow-release fertilizer would reduce the demand for commercial agricultural fertilizers to meet crop growth expectations, and reduce the total amount of phosphates contained in agricultural runoff.

Amending agricultural soils with biochars has the potential for carbon sequestration. Although the production of biochars includes producing syngas, if approximately 40% of biochars are returned to soil, the greenhouse gas emissions of the production and usage of biochars is neutral, turning the carbon cycle renewable (Yang et al. 2016). Applying biochars would provide a permanent offset in CO_2 emissions (Sohi et al. 2010), and allow carbon that would otherwise be released into the atmosphere to remain in soil.

In addition to carbon sequestration, biochars could amend the pH of acidic soils. Huang et al. (2012) noted that most biochars are alkaline, even if their source material is acidic. This alkalinity comes from organic anion bases from nutrients, which are condensed during pyrolysis. The biochars produced from pyrolysis have a higher concentration of these bases, and thus a pH >7. As cornstalk is naturally exposed to more nutrients and is a known nutrient sink in agricultural fields, the pH is likely well above 7. Sawdust may contain less nutrients due to less exposure to fertilizer and other nutrients found in agricultural fields, but is still expected to be alkaline. Adding these biochars to acidic soils could amend the pH and allow for better conditions for plant growth.

6 CONCLUSION

Engineered biochar s derived from sawdust and cornstalk residue have the potential for use as (a) an effective remediation tools for the removal of phosphates from agricultural runoff and (b) an agricultural soil amendment, acting as a fertilizer to increase crop growth. Unmodified cornstalk biochar released phosphates into solution, and could be used on its own as a soil amendment to increase crop growth. Engineered magnesium-oxide biochar nanocomposites displayed high phosphate adsorption capacities, showing essentially complete removal at 30 mg/L phosphate concentration. Sawdust-based magnesium-oxide biochar displayed adsorption characteristics that correlated well with both Langmuir and Freundlich isotherm models, with Langmuir isotherm model showing slightly higher correlation, suggesting linear monolayer physiorption as the main mechanism for phosphate adsorption. However, cornstalk residue-based magnesium oxide biochar did not match either isotherm models studied particularly well. Other adsorption mechanisms are likely major contributors to the adsorption properties of the corn-based biochar. The source material chemical and physical compositions possibly play a major role in this deviation from typical physisorption isotherm models.

Future research should include characterizing and verifying the physical and chemical properties discussed in previous sections, as the material characterization was limited in this experiment. These include the pH, surface area, porosity, surface charge, material composition, bio-oil and syngas production, magnesium oxide nanocrystalline structures, and complexation reactions forming magnesium-phosphate complexes on the biochar surface. Possible research directions could include the use of phosphorus-laden biochars as a slow-release fertilizer, column testing to determine the potential characteristics of a biochar filterbed, the use of an aggregate aqueous solution to mimic agricultural fertilizer and potential phosphate adsorption inhibitors, or the use of different raw materials or treatment methods in the biochar production process.

7 REFERENCES

Ahmad, M., Lee, S. S., Dou, X., Mohan, D., Sung, J.-K., Yang, J. E., and Ok, Y. S. (2012). "Effects of pyrolysis temperature on soybean stover- and peanut shell-derived biochar properties and TCE adsorption in water." *Bioresource technology*, 118, 536–44.

Ahmad, M., Rajapaksha, A. U., Lim, J. E., Zhang, M., Bolan, N., Mohan, D., Vithanage, M., Lee, S. S., and Ok, Y. S. (2014). "Biochar as a sorbent for contaminant management in soil and water: A review." *Chemosphere*, Elsevier Ltd, 99, 19–23.

Anawar, H. M., Akter, F., Solaiman, Z. M., and Strezov, V. (2015). "Biochar: An Emerging Panacea for Remediation of Soil Contaminants from Mining, Industry and Sewage Wastes." *Pedosphere*, Soil Science Society of China, 25(5), 654–665.

Atkinson, C. J., Fitzgerald, J. D., and Hipps, N. A. (2010). "Potential mechanisms for achieving agricultural benefits from biochar application to temperate soils: A review." *Plant and Soil*, 337(1), 1–18.

Beesley, L., and Dickinson, N. (2010). "Carbon and trace element mobility in an urban soil amended with green waste compost." *Journal of Soils and Sediments*, 10(2), 215–222.

Beesley, L., Moreno-Jiménez, E., Gomez-Eyles, J. L., Harris, E., Robinson, B., and Sizmur, T. (2011). "A review of biochars' potential role in the remediation, revegetation and restoration of contaminated soils." *Environmental Pollution*, Elsevier Ltd, 159(12), 3269–3282.

Beesley, L., Moreno-Jiminez, E., and Gomez-Eyles, J. L. (2010). "Effects of biochar and greenwaste compost amendments on mobility, bioavailability and toxicity of inorganic and organic contaminants in a multi-element polluted soil." *Environmental Pollution*, 158(6), 2282–2287.

Biederman, L. A., and Stanley Harpole, W. (2013). "Biochar and its effects on plant productivity and nutrient cycling: A meta-analysis." *GCB Bioenergy*, 5(2), 202–214.

Boehm, H. P. (1994). "Some aspects of the surface chemistry of carbon blacks and other carbons." *Carbon*, 32(5), 759–769.

Cao, X., Ma, L., Liang, Y., Gao, B., and Harris, W. (2011). "Simultaneous immobilization of lead and atrazine in contaminated soils using dairy-manure biochar." *Environmental science & technology*, 45(11), 4884–4889.

Carpenter, S., Caraco, N. F., Correll, D. L., Howarth, R. W., Sharpley, A. N., and Smith, V. H. (1998). "Nonpoint pollution of surface waters with phosphorus and nitrogen." *Issues Ecol.*, 3(January 1998), 1 – 12.

Chen, B., Chen, Z., and Lv, S. (2011). "A novel magnetic biochar efficiently sorbs organic pollutants and phosphate." *Bioresource Technology*, Elsevier Ltd, 102(2), 716–723.

Chen, B., Zhou, D., and Zhu, L. (2008). "Transitional adsorption and partition of nonpolar and polar aromatic contaminants by biochars of pine needles with different pyrolytic temperatures." *Environmental Science and Technology*, 42(14), 5137–5143.

Daniel, T. C., Sharpley, a. N., and Lemunyon, J. L. (1998). "Agricultural Phosphorus and Eutrophication: A Symposium Overview." *Journal of Environment Quality*, 27(2), 251.

De-Bashan, L. E., and Bashan, Y. (2004). "Recent advances in removing phosphorus from wastewater and its future use as fertilizer (1997-2003)." *Water Research*, 38(19), 4222–4246.

Diaz, R. J., and Rosenberg, R. (2008). "Spreading dead zones and consequences for marine ecosystems." *Science*, 321(5891), 926–929.

Ding, Z., Hu, X., Wan, Y., Wang, S., and Gao, B. (2015). "Removal of lead, copper, cadmium, zinc, and nickel from aqueous solutions by alkali-modified biochar: Batch and column tests." *Journal of Industrial and Engineering Chemistry*, The Korean Society of Industrial and Engineering Chemistry, 33, 239–245.

Dodds, W. K., Bouska, W. W., Eitzmann, J. L., Pilger, T. J., Pitts, K. L., Riley, A. J., Schloesser, J. T., and Thornbrugh, D. J. (2009). "Eutrophication of U.S. freshwaters: analysis of potential economic damages." *Environmental science & technology*, 43(1), 12–19.

Dong, X., Ma, L. Q., and Li, Y. (2011). "Characteristics and mechanisms of hexavalent chromium removal by biochar from sugar beet tailing." *Journal of hazardous materials*, 190(1-3), 909–15.

Dooley, S. R., and Treseder, K. K. (2012). "The effect of fire on microbial biomass: A meta-analysis of field studies." *Biogeochemistry*, 109(1-3), 49–61.

Fellet, G., Marchiol, L., Delle Vedove, G., and Peressotti, A. (2011). "Application of biochar on mine tailings: effects and perspectives for land reclamation." *Chemosphere*, 83(9), 1262–7.

Glaser, B., Lehmann, J., and Zech, W. (2002). "Ameliorating physical and chemical properties of highly weathered soils in the tropics with charcoal - A review." *Biology and Fertility of Soils*, 35(4), 219–230.

González, J. F., Encinar, J. M., Canito, J. L., Sabio, E., and Chacón, M. (2003). "Pyrolysis of cherry stones: Energy uses of the different fractions and kinetic study." *Journal of Analytical and Applied Pyrolysis*, 67(1), 165–190.

Guo, M., and Bi, J. (2015). "Pyrolysis Characteristics of Corn Stalk with Solid Heat Carrier." 10(3), 3839–3851.

Hach. (2014). "Method 8048, Ascorbic Acid method for Phosphorus , Reactive (Orthophosphate)." 1–8.

Han, L., Xue, S., Zhao, S., Yan, J., Qian, L., and Chen, M. (2015). "Biochar supported nanoscale iron particles for the efficient removal of methyl orange dye in aqueous solutions." *PLoS ONE*, 10(7), 1–15.

Huang, Y. W., Chen, W. F., Sun, D. Q., Guan, X. C., Zhang, W. M., Yu, L., Gao, J. P., and Meng, J. (2012). "Research on Physical and Chemical Properties of Different Biochars." *Advanced Materials Research*, 518-523, 807–816.

Jones, D. L., Edwards-Jones, G., and Murphy, D. V. (2011). "Biochar mediated alterations in herbicide breakdown and leaching in soil." *Soil Biology and Biochemistry*, 43(4), 804–813.

Kammen, D. M., and Lew, D. J. (2005). "Review of Technologies for the Production and Use of Charcoal." *Renewable and Appropriate Energy Laboratory Report*, 1–19.

Kong, H., He, J., Gao, Y., Wu, H., and Zhu, X. (2011). "Cosorption of Phenanthrene and Mercury(II) from Aqueous Solution by Soybean Stalk-Based Biochar." *Journal of Agricultural and Food Chemistry*, 59(22), 12116–12123.

Kookana, R. S., Sarmah, A. K., Van Zwieten, L., Krull, E., and Singh, B. (2011). *Biochar application to soil. agronomic and environmental benefits and unintended consequences*. *Advances in Agronomy*, Elsevier Inc.

Krishnan, K. A., and Haridas, A. (2008). "Removal of phosphate from aqueous solutions and sewage using natural and surface modified coir pith." *Journal of Hazardous Materials*, 152(2), 527–535.

Kuppusamy, S., Thavamani, P., Megharaj, M., Venkateswarlu, K., and Naidu, R. (2016). "Agronomic and remedial benefits and risks of applying biochar to soil: Current knowledge and future research directions." *Environment International*, Elsevier Ltd, 87, 1–12.

Laghari, M., Hu, Z., Mirjat, M. S., Xiao, B., Tagar, A. A., and Hu, M. (2015). "Fast pyrolysis biochar from sawdust improves the quality of desert soils and enhances plant growth." *Journal of the Science of Food and Agriculture*, (November 2014).

Lehmann, J., and Joseph, S. (Eds.). (2009). *Biochar for Environmental Management*. Earthscan.

Lima, I. M., Boateng, A. A., and Klasson, K. T. (2010). "Physicochemical and adsorptive properties of fast-pyrolysis bio-chars and their steam activated counterparts." *Journal of Chemical Technology & Biotechnology*, John Wiley & Sons, Ltd., 85(11), 1515–1521.

Mohan, D., Sarswat, A., Ok, Y. S., and Pittman, C. U. (2014). "Organic and inorganic contaminants removal from water with biochar, a renewable, low cost and sustainable adsorbent - A critical review." *Bioresource Technology*, Elsevier Ltd, 160, 191–202.

Mubarik, S., Saeed, A., Athar, M. M., and Iqbal, M. (2014). "Characterization and mechanism of the adsorptive removal of 2,4,6-trichlorophenol by biochar prepared from sugarcane baggase." *Journal of Industrial and Engineering Chemistry*, The Korean Society of Industrial and Engineering Chemistry, 33, 115–121.

Namgay, T., Singh, B., and Singh, B. P. (2010). "Influence of biochar application to soil on the availability of As, Cd, Cu, Pb, and Zn to maize (Zea mays L.)." *Soil Research*.

NOAA. (2015). "2015 Gulf of Mexico dead zone ' above average ." *National Oceanic and Atmospheric Administration (NOAA)*, <http://www.noaanews.noaa.gov/stories2015/080415-gulf-of-mexico-dead-zone-above-average.html>.

Ohio EPA. (2015). "Ohio Algae Information for Recreational Waters." *Ohio Environmental Protection Agency (EPA)*, <http://epa.ohio.gov/habalgae.aspx#147744472-basics>.

Okimori, Y., Ogawa, M., and Takahashi, F. (n.d.). "Potential of Co2 emission reductions by carbonizing biomass waste from industrial tree plantation in South Sumatra, Indonesia." *Mitigation and Adaptation Strategies for Global Change*, 8(3), 261–280.

ORSANCO. (2015). *Ohio River HAB Event*. Ohio River Valley Water Sanitation Comission (ORSCANO). October 2015 Presentaitons, Agenda Item 10c.

Park, J. H., Choppala, G. K., Bolan, N. S., Chung, J. W., and Chuasavathi, T. (2011). "Biochar reduces the bioavailability and phytotoxicity of heavy metals." *Plant and Soil*, 348(1), 439–451.

Peacocke, G. V. C. (1994). "Ablative pyrolysis of biomass." *Science*, 7(1-6), 147–154.

Qayyum, M. F., Ashraf, I., Abid, M., and Steffens, D. (2015). "Effect of biochar, lime, and compost application on phosphorus adsorption in a Ferralsol." *Journal of Plant Nutrition and Soil Science*, 576–581.

Qian, K., Kumar, A., Zhang, H., Bellmer, D., and Huhnke, R. (2015). "Recent advances in utilization of biochar." *Renewable and Sustainable Energy Reviews*, Elsevier, 42, 1055–1064.

Rabalais, N. N., Turner, R. E., Díaz, R. J., and Justić, D. (2009). "Global change and eutrophication of coastal waters." *ICES Journal of Marine Science*, 66(7), 1528–1537.

Roberts, D. A., Paul, N. A., Cole, A. J., and de Nys, R. (2015). "From waste water treatment to land management: Conversion of aquatic biomass to biochar for soil amelioration and the fortification of crops with essential trace elements." *Journal of Environmental Management*, Elsevier Ltd, 157, 60–68.

Smart Fertilizer. (2016). "Fertilizer Analysis and Comparison." <http://www.smart-fertilizer.com/articles/fertilizer-composition> (Apr. 27, 2016).

Sohi, S. P., Krull, E., Lopez-Capel, E., and Bol, R. (2010). "A review of biochar and its use and function in soil." *Advances in Agronomy*, 105(1), 47–82.

Sun, L., Chen, D., Wan, S., and Yu, Z. (2015). "Performance, kinetics, and equilibrium of methylene blue adsorption on biochar derived from eucalyptus saw dust modified with citric, tartaric, and acetic acids." *Bioresource Technology*, Elsevier Ltd, 198, 300–308.

Tinwala, F., Mohanty, P., Parmar, S., Patel, A., and Pant, K. K. (2015). "Intermediate pyrolysis of agro-industrial biomasses in bench-scale pyrolyser: Product yields and its characterization." *Bioresource Technology*, Elsevier Ltd, 188, 258–264.

Tong, X. J., Li, J. Y., Yuan, J. H., and Xu, R. K. (2011). "Adsorption of Cu(II) by biochars generated from three crop straws." *Chemical Engineering Journal*, 172(2-3), 828–834.

Trakal, L., Veselská, V., Šafařík, I., Vítková, M., Číhalová, S., and Komárek, M. (2016). "Lead and cadmium sorption mechanisms on magnetically modified biochars." *Bioresource Technology*, 203, 318–324.

US EPA. (2015). "Drinking Water Health Advisory for the Cyanobacterial Microcystin Toxins." (June).

West Virginia BPD. (2015). "DHHR Lifts Blue-Green Algal Blooms Advisory on the Ohio River." West Virginia Department of Health and Human Resources, Bureau for Public Health.

Whitehead, W. D. J. (1980). "The construction of a transportable charcoal kiln." *Rural Technology Guide, Tropical Products Institute*, London, 1–19.

William H. Maxwell. (1976). "Stationary Source Testing of a Missouri-Type Charcoal Kiln - Midwest Research Institute."

Wood, M., Branch, P., Division, F. I., and Division, P. (2014). *Industrial charcoal making*. *FAO Forestry Paper*.

Xu, R., Xiao, S., Yuan, J., and Zhao, A. (2011). "Adsorption of methyl violet from aqueous solutions by the biochars derived from crop residues." *Bioresource technology*, 102(22), 10293–8.

Xu, T., Lou, L., Luo, L., Cao, R., Duan, D., and Chen, Y. (2012). "Effect of bamboo biochar on pentachlorophenol leachability and bioavailability in agricultural soil." *Science of the Total Environment*, 414, 727–731.

Yang, Q., Han, F., Chen, Y., Yang, H., and Chen, H. (2016). "Greenhouse gas emissions of a biomass-based pyrolysis plant in China." *Renewable and Sustainable Energy Reviews*, Elsevier, 53, 1580–1590.

Yao, Y. (2013). "Sorption of Phosphate and Other Contaminants On Biochar and Its Environmental Implications."

Yao, Y., Gao, B., Chen, J., and Yang, L. (2013a). "Engineered Biochar Reclaiming Phosphate from Aqueous Solutions: Mechanisms and Potential Application as a Slow-Release Fertilizer." *Environmental Science and Technology*, 47, 8700–8708.

Yao, Y., Gao, B., Chen, J., Zhang, M., Inyang, M., Li, Y., Alva, A., and Yang, L. (2013b). "Engineered carbon (biochar) prepared by direct pyrolysis of Mg-accumulated tomato tissues: Characterization and phosphate removal potential." *Bioresource Technology*, Elsevier Ltd, 138, 8–13.

Yao, Y., Gao, B., Inyang, M., Zimmerman, A. R., Cao, X., Pullammanappallil, P., and Yang, L. (2011). "Removal of phosphate from aqueous solution by biochar derived from anaerobically digested sugar beet tailings." *Journal of Hazardous Materials*, Elsevier B.V., 190(1-3), 501–507.

Zhang, H., Lin, K., Wang, H., and Gan, J. (2010). "Effect of Pinus radiata derived biochars on soil sorption and desorption of phenanthrene." *Environmental Pollution*, 158(9), 2821–2825.

Zhang, M., Gao, B., Yao, Y., Xue, Y., and Inyang, M. (2012). "Synthesis of porous MgO-biochar nanocomposites for removal of phosphate and nitrate from aqueous solutions." *Chemical Engineering Journal*, Elsevier B.V., 210, 26–32.

Zhang, T., Walawender, W. P., Fan, L. T., Fan, M., Daugaard, D., and Brown, R. C. (2004). "Preparation of activated carbon from forest and agricultural residues through CO2 activation." *Chemical Engineering Journal*, 105(1-2), 53–59.

8 APPENDICES

8.1 DETAILED EXPERIMENTAL METHODS

8.1.1 General materials used:

- Eppendorf Research Adjustable ES-1000 100-1000-µL pipette, with plastic tips
- Eppendorf Research Adjustable ES-100 10-100 µL pipette, with plastic tips
- Fisherbrand Disposable Plastic Pipettes (2,5,10,25 mL)
- Thermo Scientific Nunc Disposable Plastic Pipettes (2,5,10,25 mL)
- Fisherbrand Low Form Weighing Dish, Fluted Aluminum, 42mL
- Microflex, Miracle, or Perform Nirtile Powder-Free examination gloves

8.1.2 Pre-pyrolysis preparation

8.1.2.1 Materials Used:

- Oak Sawdust (from Ogonek Custom Hardwoods)
- Cornstalk Residue (from Spencerville, OH)
- Fisher 5.0M HCl
- Fisher $MgCl_2*6H_2O$ Salt
- SI-300R Orbital Shaker

8.1.2.2 Procedure:

Unmodified Biochar Preparation:

1. Break down cornstalk residue into approximately ¼”-1” pieces. This is used in all cornstalk-based biochar production.
2. Weigh appropriate amount of raw material (30.0g used in this study)
3. Rinse broken-down cornstalk residue and sawdust (separately) for 90 seconds with RO water.
4. Oven-dry raw materials at 110°C overnight.
5. Store materials in closed jars until pyrolysis.

Acid-rinsed Biochar Preparation:

1. Prepare 1L of a dilute HCl solution by mixing 100 mL of 5.0 M HCl with 900 mL of water.
2. Place 35.0g of desired raw material into a graduated cylinder with the dilute acid solution.
3. Leave raw material in the acid solution for 60 minutes. Agitate the acid bath manually with a glass stir-rod for 60 seconds every 10 minutes during the pretreatment.

4. Remove material from acid bath. Rinse thoroughly with RO water.
5. Oven-dry raw materials at 110°C overnight.
6. Store materials in closed jars until pyrolysis.

Magnesium-loaded Biochar:

1. Dissolve 80.0g of $MgCl_2*6H_2O$ into 200 mL of RO water. Mix until $MgCl_2*6H_2O$ is completely dissolved.
2. Place 10.0g of desired raw material in MgCl solution
3. Mix MgCl-raw material mixture with the SI-300R orbital shaker at 75 rpm for 2 hours.
4. Remove raw material from solution. Do not rinse with RO water
5. Oven-dry raw materials at 110°C overnight.
6. Store materials in closed jars until pyrolysis.

8.1.2.3 Data Gathered

- Mass of raw material used for each biochar production method

8.1.3 Biochar Production

8.1.3.1 Materials Used:

- Pyrolysis reactor (See Section 8.4)
- Prepared biochar raw materials (from 8.1.1)
- Unasco Nickel anti-seize tape (-268° to 1,300° C)
- Lindberg Furnace
- Industrial-grade nitrogen gas
- Coffeemate blade grinder

8.1.3.2 Procedure:

Pyrolysis Trials:

Note: See Section 8.4 for a schematic of the reactor used and the pyrolysis process.

1. Record the initial mass of the biochar being used.
2. Ensure sure pyrolysis reactor is set up in a well-ventilated area.
3. Load prepared raw material into reactor. Ensure that the packing density allows for nitrogen airflow through the reactor to the exhaust tube.
4. Wrap reactor threads in nickel anti-seize tape.
5. Close reactor. Ensure nitrogen airflow can travel through the reactor and reach the exhaust port.
6. Turn on exhaust fan for proper ventilation.
7. Turn on nitrogen flow. Pipe nitrogen through reactor at 2 L/min for 15 minutes.

8. Set furnace to 500 °C. Turn on furnace.
9. Once furnace has reached 500 °C (approximately 30 minutes), maintain heat application for 30 minutes.
10. Turn off furnace, allow reactor to cool to room temperature
11. Continue nitrogen flow for 10-15 minutes after the furnace is turned off; until smoke is no longer visible from the exhaust pipe.

Post-pyrolysis production:

1. After reactor has cooled, remove biochar from reactor.
2. Using a Coffeemate blade grinder, break down biochar materials. Use 2-3 10 second pulses, allowing the biochar powder to settle after each pulse. Repeat until a powder-like consistency is achieved
3. Weigh the final mass of biochar produced.
4. Store biochar in a closed opaque jar for future trials.

Apparent Density:

1. After biochar has been produced, fill a graduated cylinder to target volume of biochar (3 mL used in this study). Do not compact the biochar or allow the biochar to settle.
2. Record the mass of biochar required to reach the target volume.

8.1.3.3 Data Gathered:

- Initial mass of biochar, pre-pyrolysis
- Mass of biochar after pyrolysis and production.
- Known volume of a measured mass of biochar

8.1.3.4 Results:

- Biochar product yield (Eq. 4-1, section 4.3)
- Bulk density of biochars (Eq. 4-2, section 4.3)

8.1.4 Adsorption Trials

8.1.4.1 Materials Used:

- Fisher $NaH_2PO_4*H_2O$
- Fisher 50mL Centrifuge Tubes
- Big SHOT III Hybridization Oven
- BD 10mL Syringer, Luer-Lok Tip
- Corning Incoporated 28mm Syringe membrane filter (0.20 μm)
- Hach DR/890 Colorimeter

- Hach PhosVer 3 Phosphate Reagent, for 10mL samples

8.1.4.2 Procedure:

1. Prepare 1L of a 1g/L PO_4^{3-} stock solution by dissolving 1.453g of $NaH_2PO_4*H_2O$ into 1.0L of RO water. Mix until fully dissolved. Prepare appropriate dilutions of PO_4^{3-} from this stock solution.
2. For acid-rinsed and unmodified biochars, prepare a 20g/L biochar slurry with 0.8g of biochar mixed with RO water to reach a total volume of 40 mL (use the bulk densities of biochars, calculated in Section 8.1.3). MgO biochars need to be weighed for each individual trial.
3. Prepare appropriate PO_4^{3-} dilution (or RO water for negative controls). Record concentration using the Hach Colorimeter and Hach Method 8048 for Orthophosphate.
4. Prepare batch reactor by placing 40mL of phosphate solution (or RO water) and target mass of biochar (using biochar slurry or individually weighed) into 50ml centrifuge tubes. Prepare three batch reactors per experimental condition.
5. Place all reactors in Big SHOT III hybridization oven. Run adsorption isotherms with the hybridization oven at 30°C and 60 rpm for 24 hours.
6. Remove batch reactors from hybridization oven.
7. Using a 10mL syringe and 0.20 μm, filter out biochar from the liquid solution.
8. Measure final phosphate concentration using Hach Method 8048. Record two trials per sample (total of 6 data points per experimental condition).

8.1.4.3 Data Gathered:

- Mass of biochar
- Volume of solution
- Total volume (if slurry is used)
- Initial PO_4^{3-} concentration
- Final PO_4^{3-} concentration

8.1.4.4 Results:

- q (Eq 4-4, section 4.3)
- Langmuir isotherm model constants (Eq 4-5, section 4.3)
- Freundlich isotherm model constants (Eq 4-6, section 4.3)

8.2 EXPERIMENTAL MATRIX FOR ADSORPTION TRIALS[1]

Biochar Tested[2] / Liquid Used[3]	CP	CA	CMgO	SP	SA	SMgO
RO water	[0.1g]	[0.1g]	[0.1g]	[0.1g]	[0.1g]	[0.1g]
30 mg/L Phosphate	[0.1g]	[0.1g]	[0.01g] [0.02g] [0.05g] [0.1g]	[0.1g]	[0.1g]	[0.01g] [0.02g] [0.05g] [0.1g]
60 mg/L Phosphate	NT[4]	NT	[0.05g]	NT	NT	[0.05g]
150 mg/L Phosphate	NT	NT	[0.05g]	NT	NT	[0.05g]
300 mg/L Phosphate	NT	NT	[0.05g]	NT	NT	[0.05g]

Note: (1)- Batch experiments were run in triplicate, with two samples taken per batch reactor
(2)- [Masses] listed in the matrix represent mass of biochar used during an adsorption trial.
(3)- 40 mL of liquid was used with designated mass of biochar
(4)- NT – not tested

8.3 DATA AND SAMPLE CALCULATIONS

8.3.1 Biochar Yield

Biochar	Mi (g)	M (g)	y (%)
CP	30.04	10.18	33.9%
CA	35	11.40	32.6%
CMgO	10	7.16	71.6%
SP	30	7.23	24.1%
SA	35	9.74	27.8%
SMgO	10	9.10	91.0%

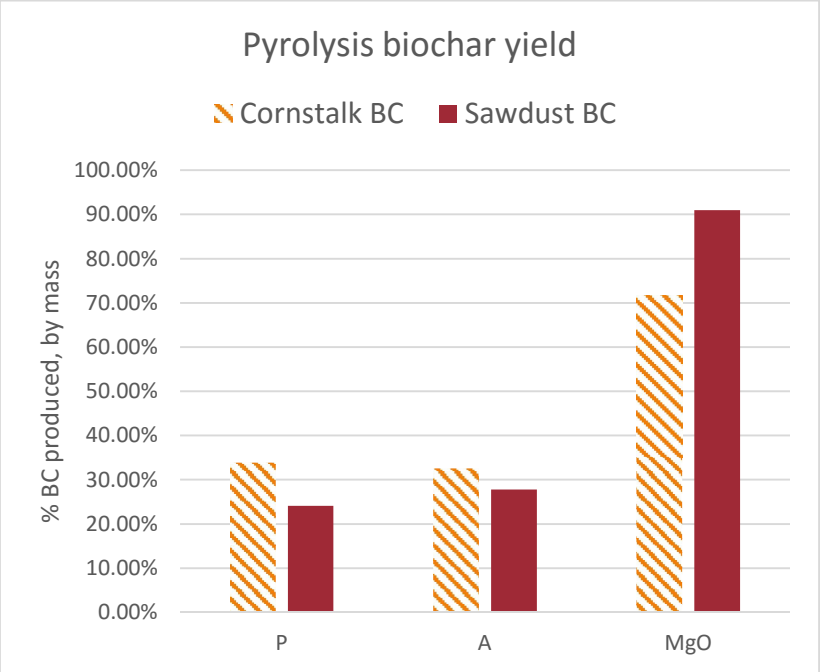

Sample Calculation:

$$y = \frac{M}{Mi} * 100$$

$$y = \frac{10.18g}{30.04g} * 100$$

$$y = 33.9\%$$

8.3.2 Bulk Density

Biochar	V (mL)	M (g)	ρ (g/L)
CP	3	0.57	188.33
CA	3	0.63	209.27
CMgO	4.5	1.28	285.53
SP	3	0.92	306.60
SA	3	1.15	384.47
SMgO	3.5	1.66	473.71

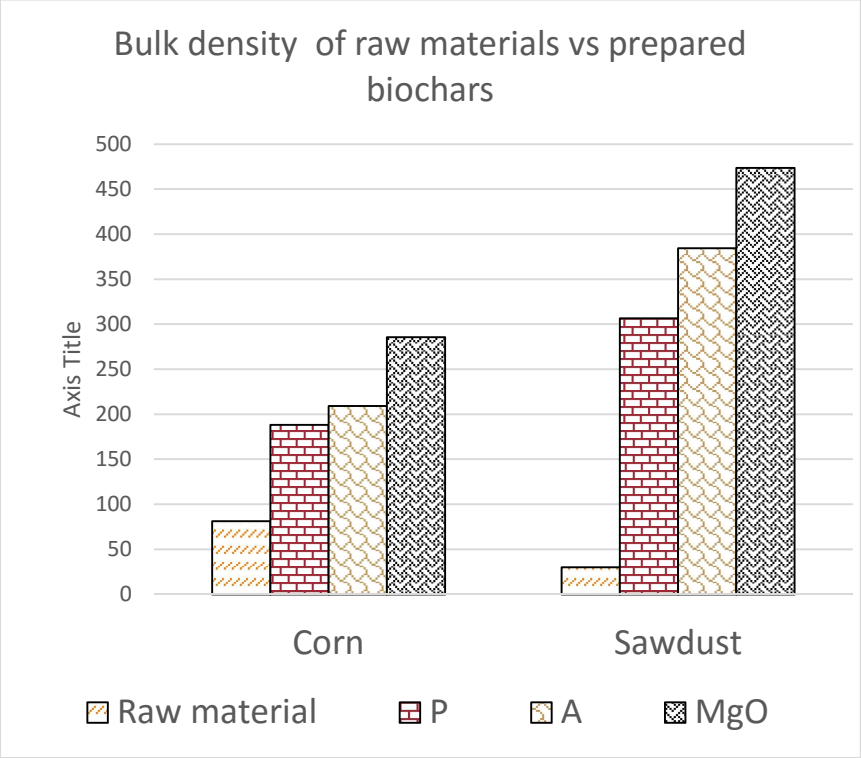

Sample Calculation:

$$\rho = \frac{m}{V}$$

$$\rho = \frac{0.57g}{3mL} \times \frac{1000mL}{1L}$$

$$\rho = 188.33\ g/L$$

8.3.3 30 mg/L Phosphate Adsorption Screen

Biochar	$[PO4]_i$ (mg/L)	[PO4] 24h (mg/L)	m Sorbent	qe, mg/g	Ceq/Ci	Removal Eff.
SP	28.15	30.17	0.1	-1.10	1.07	-7.17%
SA	28.15	28.80	0.1	-3.41	1.02	-2.32%
SMgO	31.67	0.21	0.1	12.58	0.01	99.35%
CP	28.15	34.45	0.1	-2.84	1.22	-22.39%
CA	28.15	24.35	0.1	1.71	0.87	13.49%
CMgO	31.67	0.36	0.1	12.52	0.01	98.88%

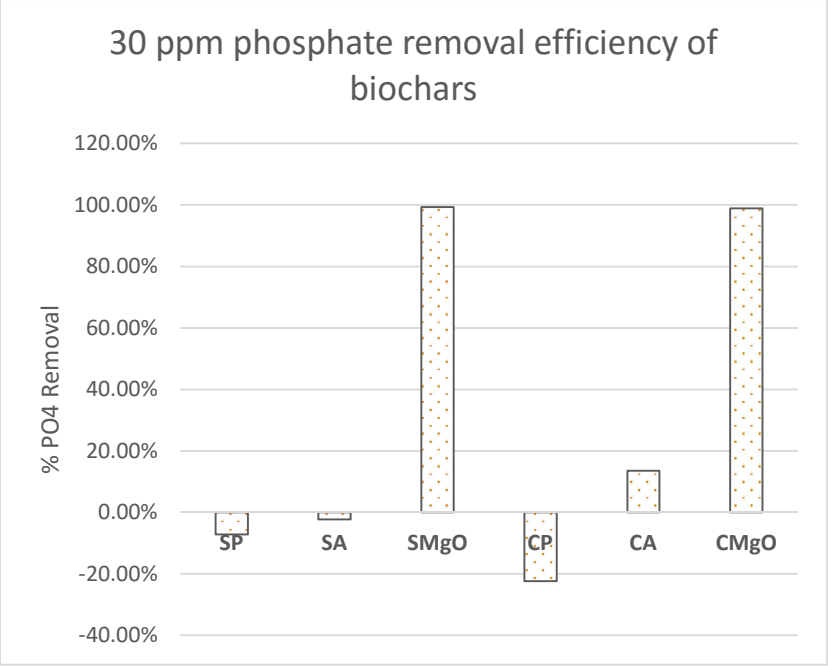

Sample Calculation:

$$e = \frac{Ci - C_{eq}}{Ci} * 100$$

$$e = \frac{28.15 \frac{mg}{L} - 30.17\ mg/L}{28.15\ mg/L} * 100$$

$$e = -7.17\%$$

8.3.4 Adsorption Trials

8.3.4.1 Sawdust

V (L)	M (g)	[PO4]i (mg/L)	[PO4] (mg/L)	qe, (mg/g)	Ce/qe	Log Ce	Log qe
0.04	0.1	31.7	0.20	12.59	0.02	-0.70	1.10
0.04	0.1	31.7	0.20	12.59	0.02	-0.70	1.10
0.04	0.1	31.7	0.20	12.59	0.02	-0.70	1.10
0.04	0.1	31.7	0.22	12.58	0.02	-0.66	1.10
0.04	0.1	31.7	0.24	12.57	0.02	-0.62	1.10
0.04	0.1	31.7	0.18	12.59	0.01	-0.74	1.10
0.04	0.05	32.7	0.74	25.59	0.03	-0.13	1.41
0.04	0.05	32.7	1.72	24.81	0.07	0.24	1.39
0.04	0.05	32.7	1.80	24.75	0.07	0.26	1.39
0.04	0.05	32.7	0.78	25.56	0.03	-0.11	1.41
0.04	0.05	32.7	1.80	24.75	0.07	0.26	1.39
0.04	0.05	32.7	1.78	24.76	0.07	0.25	1.39
0.04	0.02	32.7	11.45	42.57	0.27	1.06	1.63
0.04	0.02	32.7	11.10	43.27	0.26	1.05	1.64
0.04	0.02	32.7	10.75	43.97	0.24	1.03	1.64
0.04	0.02	32.7	10.30	44.87	0.23	1.01	1.65
0.04	0.02	32.7	10.00	45.47	0.22	1.00	1.66
0.04	0.01	32.7	17.80	59.73	0.30	1.25	1.78
0.04	0.01	32.7	18.70	56.13	0.33	1.27	1.75
0.04	0.01	32.7	17.80	59.73	0.30	1.25	1.78
0.04	0.01	32.7	19.40	53.33	0.36	1.29	1.73
0.04	0.01	32.7	18.70	56.13	0.33	1.27	1.75
0.04	0.01	32.7	18.00	58.93	0.31	1.26	1.77
0.04	0.05	32.7	0.74	25.59	0.03	-0.13	1.41
0.04	0.05	32.7	1.72	24.81	0.07	0.24	1.39
0.04	0.05	32.7	1.80	24.75	0.07	0.26	1.39
0.04	0.05	32.7	0.78	25.56	0.03	-0.11	1.41
0.04	0.05	32.7	1.80	24.75	0.07	0.26	1.39
0.04	0.05	32.7	1.78	24.76	0.07	0.25	1.39
0.04	0.05	64.3	4.10	48.14	0.09	0.61	1.68
0.04	0.05	64.3	3.76	48.41	0.08	0.58	1.68
0.04	0.05	64.3	5.20	47.26	0.11	0.72	1.67
0.04	0.05	64.3	3.56	48.57	0.07	0.55	1.69
0.04	0.05	64.3	4.24	48.02	0.09	0.63	1.68
0.04	0.05	64.3	5.12	47.32	0.11	0.71	1.68
0.04	0.05	165.7	38.00	102.16	0.37	1.58	2.01
0.04	0.05	165.7	38.20	102.00	0.37	1.58	2.01
0.04	0.05	165.7	45.80	95.92	0.48	1.66	1.98
0.04	0.05	165.7	38.00	102.16	0.37	1.58	2.01
0.04	0.05	165.7	38.60	101.68	0.38	1.59	2.01
0.04	0.05	165.7	47.80	94.32	0.51	1.68	1.97
0.04	0.05	324.0	178.00	116.80	1.52	2.25	2.07
0.04	0.05	324.0	188.00	108.80	1.73	2.27	2.04
0.04	0.05	324.0	178.00	116.80	1.52	2.25	2.07
0.04	0.05	324.0	174.00	120.00	1.45	2.24	2.08

8.3.4.2 Cornstalk

V (L)	M (g)	[PO4]i (mg/L)	[PO4] (mg/L)	qe, (mg/g)	Ce/qe	Log Ce	Log qe
0.04	0.1	31.7	0.46	12.48	0.04	-0.34	1.10
0.04	0.1	31.7	0.34	12.53	0.03	-0.47	1.10
0.04	0.1	31.7	0.33	12.53	0.03	-0.48	1.10
0.04	0.1	31.7	0.34	12.53	0.03	-0.47	1.10
0.04	0.1	31.7	0.31	12.54	0.02	-0.51	1.10
0.04	0.05	32.7	4.84	22.31	0.22	0.68	1.35
0.04	0.05	32.7	4.38	22.68	0.19	0.64	1.36
0.04	0.05	32.7	4.44	22.63	0.20	0.65	1.35
0.04	0.05	32.7	4.90	22.27	0.22	0.69	1.35
0.04	0.05	32.7	4.48	22.60	0.20	0.65	1.35
0.04	0.05	32.7	4.32	22.73	0.19	0.64	1.36
0.04	0.02	32.7	17.80	29.87	0.60	1.25	1.48
0.04	0.02	32.7	17.90	29.67	0.60	1.25	1.47
0.04	0.02	32.7	16.70	32.07	0.52	1.22	1.51
0.04	0.02	32.7	18.30	28.87	0.63	1.26	1.46
0.04	0.02	32.7	17.40	30.67	0.57	1.24	1.49
0.04	0.01	32.7	20.40	49.33	0.41	1.31	1.69
0.04	0.01	32.7	24.50	32.93	0.74	1.39	1.52
0.04	0.01	32.7	22.40	41.33	0.54	1.35	1.62
0.04	0.01	32.7	23.30	37.73	0.62	1.37	1.58
0.04	0.01	32.7	24.10	34.53	0.70	1.38	1.54
0.04	0.01	32.7	22.10	42.53	0.52	1.34	1.63
0.04	0.05	32.7	4.84	22.31	0.22	0.68	1.35
0.04	0.05	32.7	4.38	22.68	0.19	0.64	1.36
0.04	0.05	32.7	4.44	22.63	0.20	0.65	1.35
0.04	0.05	32.7	4.90	22.27	0.22	0.69	1.35
0.04	0.05	32.7	4.48	22.60	0.20	0.65	1.35
0.04	0.05	32.7	4.32	22.73	0.19	0.64	1.36
0.04	0.05	64.3	24.40	31.90	0.76	1.39	1.50
0.04	0.05	64.3	25.80	30.78	0.84	1.41	1.49
0.04	0.05	64.3	26.00	30.62	0.85	1.41	1.49
0.04	0.05	64.3	24.20	32.06	0.75	1.38	1.51
0.04	0.05	165.7	90.00	60.56	1.49	1.95	1.78
0.04	0.05	165.7	99.00	53.36	1.86	2.00	1.73
0.04	0.05	165.7	102.00	50.96	2.00	2.01	1.71
0.04	0.05	165.7	105.00	48.56	2.16	2.02	1.69
0.04	0.05	165.7	98.00	54.16	1.81	1.99	1.73
0.04	0.05	324.0	40.00	227.20	0.18	1.60	2.36
0.04	0.05	324.0	17.60	245.12	0.07	1.25	2.39
0.04	0.05	324.0	12.00	249.60	0.05	1.08	2.40
0.04	0.05	324.0	50.00	219.20	0.23	1.70	2.34
0.04	0.05	324.0	56.00	214.40	0.26	1.75	2.33
0.04	0.05	324.0	62.00	209.60	0.30	1.79	2.32
0.04	0.05	324.0	52.00	217.60	0.24	1.72	2.34
0.04	0.05	324.0	17.20	245.44	0.07	1.24	2.39
0.04	0.05	324.0	10.90	250.48	0.04	1.04	2.40
0.04	0.05	324.0	50.00	219.20	0.23	1.70	2.34
0.04	0.05	324.0	42.00	225.60	0.19	1.62	2.35
0.04	0.05	324.0	68.00	204.80	0.33	1.83	2.31

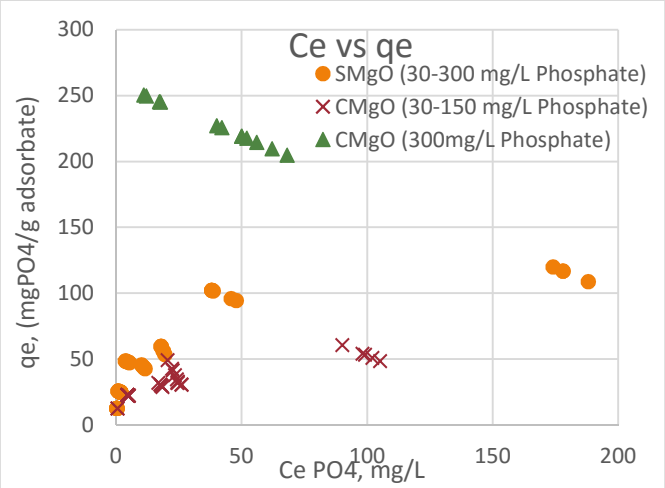

Sample Calculation

$$q = \frac{V}{M}(C_i - C_{eq})$$

$$q = \frac{40\ mL}{0.1g\ Biochar}(\frac{31.7mg}{L}Phosphate - \frac{0.46mg}{L}Phosphate)$$

$$q = 12.48\ mg\ phosphate/g\ biochar$$

8.3.4.3 Freundlich Isotherm Model

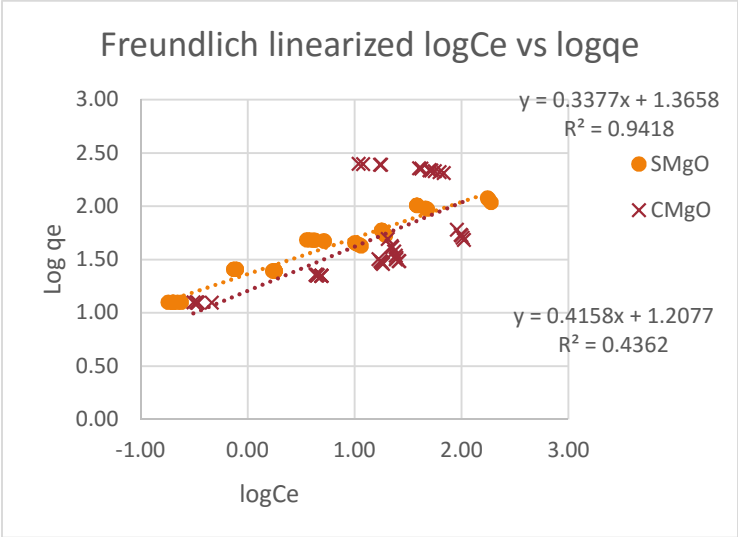

Freundlich equation: $q = KC_{eq}{}^{1/n}$

Linearized: $log\ q_A = logK_A + \left(\frac{1}{n}\right) logC_{eq}$

SMgO: $log\ q_A = 1.37 + (0.34) logC_{eq}$ CMgO: $log\ q_A = 1.21 + (0.42) logC_{eq}$

SMgO: $q = 23.22C_{eq}{}^{0.34}$ CMgO: $q = 16.13C_{eq}{}^{0.41}$

8.3.4.4 Langmuir Isotherm Model

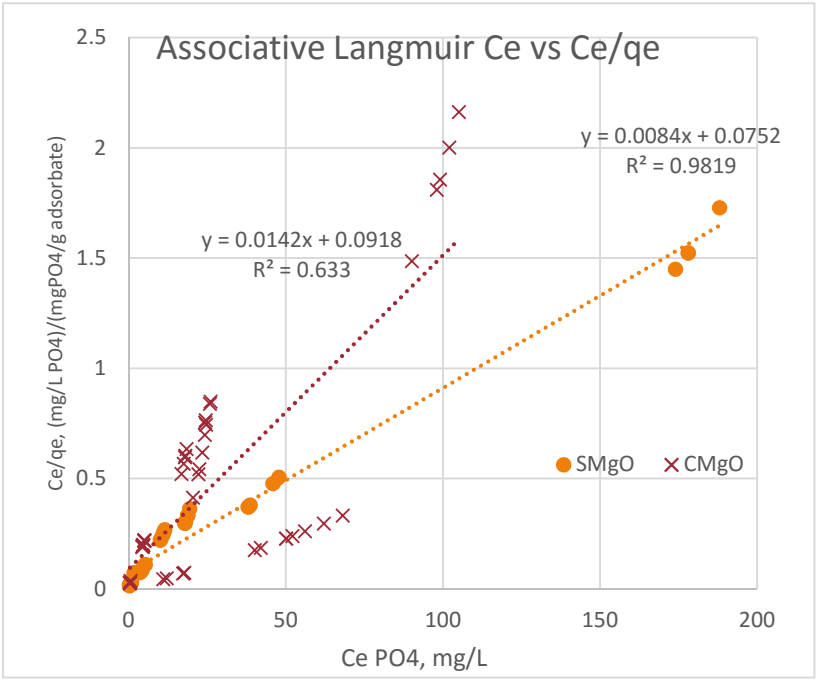

Langmuir equation: $q = \frac{Q_m b_A C_{eq}}{1+b_A C_{eq}}$

Linearized Langmuir: $\frac{C_{eq}}{q} = \frac{1}{b_A Q_M} + \frac{C_{eq}}{Q_M}$

SMgO: $\frac{C_{eq}}{q} = 0.075 + 0.0084 * C_{eq}$ CMgO: $\frac{C_{eq}}{q} = 0.092 + 0.014 * C_{eq}$

SMgO: $q = \frac{119.05*0.11*C_{eq}}{1+0.11*C_{eq}}$ CMgO: $q = \frac{70.42*0.15*C_{eq}}{1+0.15*C_{eq}}$

8.4 PYROLYSIS REACTOR

8.4.1 Detailed pyrolysis reactor:

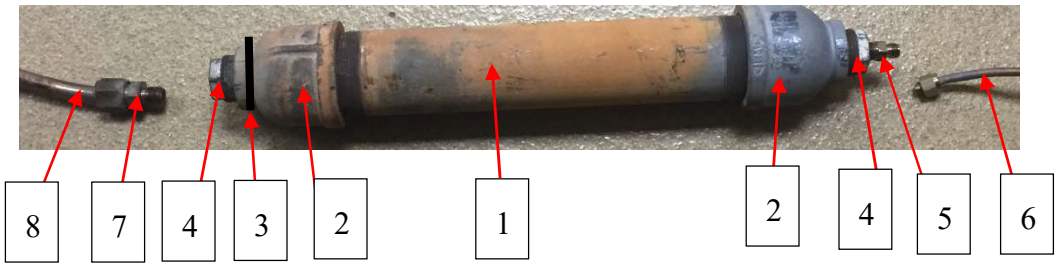

Callouts:

1. 2” I/D x12” standard-wall galvanized welded steel threaded pipe
2. 2” to 1” galvanized iron threaded pipe fitting, reducing coupling
3. Wire mesh, located inside reducing coupling
4. 1” male to ¼” female zinc-plated iron hex bushing
5. ¼” male to ¼” pipe size NPTF hex nipple, compact extreme-pressure steel
6. ¼” I/D copper tubing, nitrogen inlet
7. ¼” male to ½” pipe size NPTF hex nipple, compact extreme-pressure steel
8. ½” I/D steel tubing, exhaust for reactor

8.4.2 Pyrolysis reaction schematic